ORIGINAL RESEARCH

American Heart Association | American Stroke Association

Elongation of Long-Chain Fatty Acid Family Member 6 (Elovl6)-Driven Fatty Acid Metabolism Regulates Vascular Smooth Muscle Cell Phenotype Through AMP-Activated Protein Kinase/Krüppel-Like Factor 4 (AMPK/KLF4) Signaling

Hiroaki Sunaga, PhD;* Hiroki Matsui, PhD;* Saki Anjo, MS; Mas Risky A. A. Syamsunarno, MD, PhD; Norimichi Koitabashi, MD, PhD; Tatsuya Iso, MD, PhD; Takashi Matsuzaka, PhD; Hitoshi Shimano, MD, PhD; Tomoyuki Yokoyama, MD, PhD; Masahiko Kurabayashi, MD, PhD

***Background*—**Fatty acids constitute the critical components of cell structure and function, and dysregulation of fatty acid composition may exert diverging vascular effects including proliferation, migration, and differentiation of vascular smooth muscle cells (VSMCs). However, direct evidence for this hypothesis has been lacking. We investigated the role of elongation of long-chain fatty acid member 6 (Elovl6), a rate-limiting enzyme catalyzing the elongation of saturated and monounsaturated long-chain fatty acid, in the regulation of phenotypic switching of VSMC.

***Methods and Results*—**Neointima formation following wire injury was markedly inhibited in Elovl6-null (Elovl6$^{-/-}$) mice, and cultured VSMCs with siRNA-mediated knockdown of Elovl6 was barely responsive to PDGF-BB. Elovl6 inhibition induced cell cycle suppressors p53 and p21 and reduced the mammalian targets of rapamycin (mTOR) phosphorylation and VSMC marker expression. These changes are ascribed to increased palmitate levels and reduced oleate levels, changes that lead to reactive oxygen species (ROS) production and resulting AMP-activated protein kinase (AMPK) activation. Notably, Elovl6 inhibition robustly induced the pluripotency gene Krüppel-like factor 4 (KLF4) expression in VSMC, and KLF4 knockdown significantly attenuated AMPK-induced phenotypic switching of VSMC, indicating that KLF4 is a bona fide target of AMPK.

***Conclusions*—**We demonstrate for the first time that dysregulation of Elovl6-driven long-chain fatty acid metabolism induces phenotypic switching of VSMC via ROS production and AMPK/KLF4 signaling that leads to growth arrest and downregulation of VSMC marker expression. The modulation of Elovl6-mediated cellular processes may provide an intriguing approach for tackling atherosclerosis and postangioplasty restenosis. **(*J Am Heart Assoc*. 2016;5:e004014 doi: 10.1161/JAHA.116.004014)**

Key Words: Elovl6 • fatty acid • neointimal hyperplasia • proliferation • smooth muscle cell

Phenotypic modulation of vascular smooth muscle cells (VSMCs) is a critical process that regulates the progression of proliferative vascular disease including atherosclerosis and postangioplasty restenosis.[1-4] There have been extensive studies demonstrating that various growth factors, such as platelet-derived growth factor (PDGF) and fibroblast growth factor-2, promote phenotypic switching characterized by the downregulation of expression of differentiation marker genes such as smooth muscle α-actin (SMα-actin) and smooth muscle myosin heavy chain and the induction of proliferative capacity

From the Department of Laboratory Sciences, Gunma University Graduate School of Health Sciences, Maebashi, Japan (H. Sunaga, H.M., S.A., T.Y.); Department of Medicine and Biological Sciences, Gunma University Graduate School of Medicine, Maebashi, Japan (H. Sunaga, M.R.A.A.S., N.K., T.I., M.K.); Department of Biochemistry, Faculty of Medicine Universitas Padjadjaran, Jatinangor, Indonesia (M.R.A.A.S.); Department of Internal Medicine (Endocrinology and Metabolism), Faculty of Medicine, University of Tsukuba, Japan (T.M., H. Shimano); Graduate School of Comprehensive Human Sciences International Institute for Integrative Sleep Medicine (WPI-IIIS), Tsukuba, Japan (H. Shimano).

Accompanying Data S1, Figures S1 through S10, and Tables S1 and S2 are available at http://jaha.ahajournals.org/content/5/12/e004014/DC1/embed/inline-supplementary-material-1.pdf

*Dr Sunaga and Dr Matsui contributed equally to this work.

Correspondence to: Tomoyuki Yokoyama, MD, PhD, Department of Laboratory Sciences, Gunma University Graduate School of Health Sciences, 3-39-22, Showa-machi, Maebashi 371-8514, Japan. E-mail: tyokoyama@gunma-u.ac.jp and Masahiko Kurabayashi, MD, PhD, Department of Medicine and Biological Sciences, Gunma University Graduate School of Medicine, 3-39-15, Showa-machi, Maebashi 371-8511, Japan. E-mail: mkuraba@gunma-u.ac.jp

Received August 23, 2016; accepted October 17, 2016.

and proinflammatory gene expression.[2,5] There is now evidence that a significant fraction of VSMC within atherosclerotic plaques and cholesterol-loaded cultured VSMC express markers of macrophages and mesenchymal stem cells as well as myofibroblasts.[6-8] These findings argue that phenotypic switching of VSMC is more dynamically regulated than previously noted, and altered lipid metabolism within VSMC markedly contributes to phenotypic transitions of VSMC.

Elongation and desaturation are central steps in the de novo synthesis of long-chain fatty acids (LCFAs) that determine their function and metabolic fate. The elongation of LCFA family member 6 (Elovl6) is by a rate-limiting enzyme that mediates the elongation reaction of palmitate (C16:0) to stearate (C18:0), and stearoyl-CoA desaturase (SCD) catalyzes the conversion of stearate to oleate (C18:1 n-9).[9] Mice deficient in Elovl6 (Elovl6$^{-/-}$) are protected against diet-induced insulin resistance despite their hepatosteatosis and obesity being similar to that in wild-type (WT) mice.[10] A more recent study reported that an atherogenic high-fat diet induced hepatic inflammation, oxidative damage, and fibrosis in the liver, the hallmark features of nonalcoholic steatosis (NASH),[11] but these were attenuated in Elovl6$^{-/-}$ mice. Furthermore, Elovl6 deficiency in macrophages ameliorated foam cell formation.[12] We previously demonstrated that Elovl6 inhibition in alveolar type II epithelial cells leads to severe pulmonary fibrosis.[13] These findings suggest that Elovl6-driven LCFA metabolism regulates a plethora of cellular function. However, VSMC phenotype in Elovl6$^{-/-}$ mice remains unknown.

In the present study we investigated the effects of Elovl6 deficiency on VSMC phenotype in Elovl6$^{-/-}$ mice and in cultured human aortic smooth muscle cells (HASMC) with small interfering RNA (siRNA)-mediated Elovl6 knockdown. Our findings reveal that Elovl6 inhibition exerts profound effects on VSMC phenotype through an activation of AMP-activated protein kinase (AMPK)/Krüppel-like factor 4 (KLF4) signaling and strongly suggest a previously unrecognized mechanistic link between intracellular LCFA composition and VSMC phenotype.

Methods

Animal Model

C57BL/6 strain (WT) mice and Wistar rats were purchased from CLEA Japan Inc. Elovl6$^{-/-}$ mice were a kind gift from Dr H. Shimano (Tsukuba University). These mice were intercrossed into Elovl6$^{-/-}$ or Elovl6$^{-/+}$ mice. Littermates were genotyped by PCR. The femoral artery of 10- to 12-week-old male WT mice (n=24, 24-28 g) and Elovl6$^{-/-}$ mice (n=23, 22-26 g) was injured with a wire, as previously described,[14] with some modifications.[15] Briefly, a straight spring wire (0.38 mm in diameter, Cook Medical, Bloomington, IN) was inserted into the right femoral artery and pushed forward toward the iliac artery. The wire was left in place for 1 minute to denude and dilate the artery and then was removed. Blood flow was reconstituted after ligation of the profunda femoris branch. Mice were sacrificed 14 days after this injury, and the femoral arteries were isolated. Uninjured femoral arteries were isolated from sham controls. The carotid artery of rats was injured with a balloon as described previously.[16] See Data S1 for further details. Animal experiments using these mice were approved by and performed according to the guidelines of the Committee of Experimental Animal Research of Gunma University (Permit Number: 10-019).

Cell Culture

VSMCs from the human aorta (HASMC) were purchased from Kurabo Ltd (New York, NY). See Data S1 for further details.

RNA Isolation and Quantitative Real-Time Reverse Transcription (qRT-PCR)

Total RNA was extracted from the mouse aorta and cultured HASMC using ISOGEN regent (Takara Bio, Shiga, Japan) according to the manufacturer's protocol. See Data S1 for further details. All primer sequences are shown in Tables S1 and S2.

Recombinant Adenovirus

Adenoviruses expressing LacZ (Ad-LacZ) or Elovl6 (Ad-Elovl6) were generated as described previously.[17] HASMC were infected with Ad-Elovl6 or Ad-LacZ at a multiplicity of infection of 20 for 48 hours in preparation for the next experiments.

Elongase Activity

Microsomal fatty acid elongation activity was assayed by measuring the incorporation of [2-^{14}C]malonyl-CoA (Perkin Elmer, Shelton, CT) into exogenous acyl-CoAs as described previously.[10,13]

[^{3}H]Thymidine Uptake

The uptake of radiolabeled [^{3}H]thymidine (Perkin Elmer, Shelton, CT) was assayed as described previously,[18] with some modifications. See Data S1 for further details.

Scratch Wound Healing Assay

The measurement of migration by the scratch mobility assay was performed as described previously.[19] See Data S1 for further details.

Boyden Chamber Assay

The Boyden chamber assay was performed as previously described.[19] See Data S1 for further details.

Fatty Acid Composition

Lipids from the mouse aorta and HASMC were extracted using the Bligh and Dyer method as described previously.[20] See Data S1 for further details.

Quantitation of ROS Measurement

For the quantitation of ROS levels, we used Hydrogen Peroxide/Peroxidase Assay Kit, Fluorometric (Cell Biolabs, San Diego, CA) according to the manufacturer's protocol. Red fluorescence (excitation 550 nm; emission 590 nm) was detected by microplate reader (Perkin Elmer, EnSpire, Shelton, CT).

Statistical Analysis

All data are shown as the mean±standard error of the mean (SEM). A 2-group comparison was performed using the Mann-Whitney U-test or unpaired Student t test, and a multiple-group comparison was performed by a 1-way ANOVA with Steel-Dwass or Tukey-Kramer multiple comparison tests. A $P<0.05$ was considered significant.

Results

Elovl6 Expression in Neointimal VSMC in Uninjured and Injured Femoral Artery in Wild-Type Mice

A mouse wire-injury model, in which a straight spring wire was inserted into the femoral artery to denude and dilate the artery, was used in the present study. Immunohistochemistry revealed modest but discernible staining for Elovl6 in the medial layer of the uninjured femoral artery in WT mice. In contrast, the femoral artery 14 days after wire injury showed prominent positive staining for Elovl6 in the hypertrophic neointimal layer, in which SMα-actin-positive cells accumulated. Elovl6 staining was only modestly detected in the tunica media but was clearly detected in perivascular adipose tissue (Figure 1A).

Mice Deficient in Elovl6 Display Reduced Neointima Formation After Vascular Injury

The femoral artery of Elovl6$^{-/-}$ mice was subjected to wire injury to compare the neointima formation between WT and Elovl6$^{-/-}$ mice. Hematoxylin-eosin (H&E) and elastica van Gieson (EVG) staining showed that the thickness of the medial layer of uninjured femoral artery appeared thinner in Elovl6$^{-/-}$ mice compared with that in WT mice. Immunohistochemistry revealed that neointima formation was markedly inhibited in Elovl6$^{-/-}$ mice compared to WT mice, as assessed by H&E and EVG (Figure 1A). In addition, the semiquantitative intima/media (I/M) ratio and percentage stenosis assessment demonstrated that I/M ratio and percentage stenosis were significantly lower in Elovl6$^{-/-}$ mice than in WT mice (Figure 1B). Furthermore, immunofluorescent Ki-67 staining, a cell proliferation marker,[21] showed that neointima of Elovl6$^{-/-}$ mice had significantly fewer cells positive for Ki-67 than a similar region in WT mice (Figure 1C). These results suggested that the knockout of Elovl6 inhibits neointima formation by repressing VSMC proliferation.

Immunohistochemistry of a rat carotid subjected to balloon injury confirmed the induction of Elovl6 expression in neointimal VSMC (Figure 1D). We also examined the expression of Elovl6 in the human coronary artery obtained by autopsy. Distinct immunoreactivity for Elovl6 was detected in the medial layer and diffuse intimal thickening area, in which SMα-actin appears to be more strongly expressed (Figure S1).

Elovl6 Knockdown Reduces VSMC Proliferation and Migration

To examine the role of Elovl6 in the regulation of VSMC proliferation and migration, Elovl6 was silenced by siRNA in cultured HASMC. We first verified that Elovl6 mRNA expression was efficiently downregulated (<1% of control si green fluorescent protein [GFP]-transfected cell, $P<0.01$) as assessed by qRT-PCR, and elongase activity was reduced to 66% compared with GFP siRNA (siGFP)-transfected cells ($P<0.05$) (Figure 2A). We then examined the effects of Elovl6 knockdown on DNA synthesis by using [^{3}H]thymidine incorporation assay. In Elovl6 siRNA (siElovl6)-transfected HASMC, the incorporation of [^{3}H]thymidine was markedly reduced compared with that in siGFP-transfected control HASMC (Figure 2B). In order to confirm these results, we generated an adenovirus expressing Elovl6 (Ad-Elovl6) (Figure S2). The results obtained showed that the overexpression of Elovl6 increased the incorporation of [^{3}H]thymidine to a similar extent as PDGF-BB treatment (Figure 2B). PDGF-BB-induced incorporation as well as baseline levels of [^{3}H]thymidine incorporation were markedly diminished in siElovl6-transfected HASMC (Figure 2B). These results suggested that Elovl6 had a marked impact on VSMC proliferation at baseline and played an indispensable role in mitogenic response elicited by PDGF-BB. Together with the induction of Elovl6 gene expression by PDGF-BB (Figure S3), these results suggested that Elovl6-mediated fatty acid metabolism serves an intracellular cue for the proliferative response of VSMC to PDGF-BB stimulation. Effects of Elovl6 on VSMC migration

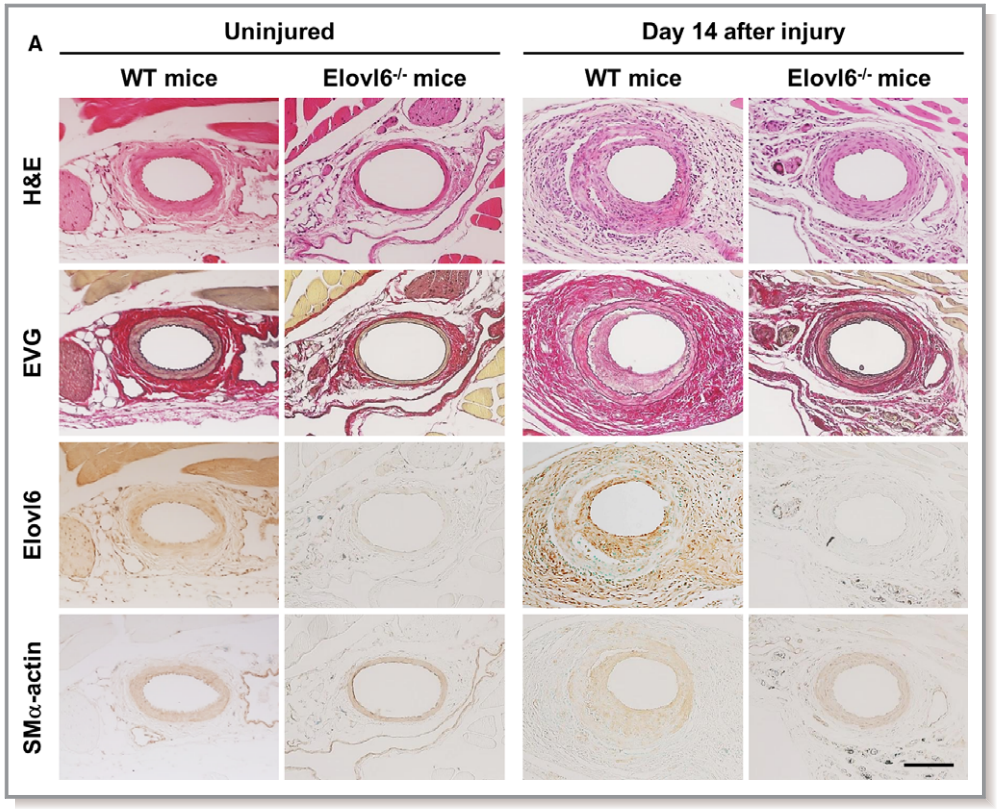

Figure 1. Neointimal hyperplasia after mechanical vascular injury is reduced in Elovl6$^{-/-}$ mice. A, Representative section of H&E staining, EVG staining, and immunohistochemical staining with Elovl6 and SMα-actin antibodies in mouse femoral artery 14 days after wire injury. The femoral arteries of 10- to 12-week-old male WT mice and Elovl6$^{-/-}$ mice were injured with a wire. The expression of Elovl6 was colocalized with SMα-actin-positive cells in WT mice. The inhibition of neointimal hyperplasia was significantly greater in Elovl6$^{-/-}$ mice than in WT mice. Scale bar=200 μm. B, The I/M ratio (left) and percentage stenosis area (right) were significantly lower in Elovl6$^{-/-}$ mice (n=9) than in WT mice (n=10). C, Representative immunofluorescence staining with a Ki-67 antibody (red) and DAPI (blue), and the number of Ki-67-positive cells per high-power field in wire-injured artery sections. The number of Ki-67-positive cells was markedly lower in Elovl6$^{-/-}$ mice (n=9) than in WT mice (n=10). Scale bar=200 μm. D, Representative sections with H&E staining, EVG staining, and immunohistochemical staining with Elovl6 and SMα-actin antibodies in the rat carotid artery subjected to balloon injury. Eight-week-old male Wistar rats were injured with a 2F balloon catheter. The expression of Elovl6 was colocalized with SMα-actin-positive cells in the uninjured WT rat carotid, and increased in the neointimal area of the balloon-injured rat carotid. Scale bar=200 μm. All values are represented as the means. *P<0.05, measured by the Mann-Whitney U-test (B) or the Student t test (C). DAPI indicates 4′,6-diamidino-2-phenylindole; Elovl6, elongation of long-chain fatty acid family member 6; EVG, elastica van Gieson; H&E, hematoxylin-eosin; I/M, intima/media; SMα-actin, smooth muscle α-actin; WT, wild-type C57BL/6.

were examined using scratch wound healing assay. Inhibition of Elovl6 in HASMC resulted in a significant decrease in migration activity as determined by Boyden chamber assay (Figure 2C).

Knockdown or Overexpression of Elovl6 Affects VSMC Marker Gene Expression

Because proliferation, migration, and differentiation are orchestrated through a shared cellular program, we determined whether Elovl6 was also involved in VSMC differentiation. We found that siRNA-mediated knockdown of Elovl6 in cultured HASMC and the disruption of the Elovl6 gene in mice reduced mRNA and protein expression levels of the SMα-actin and smooth muscle protein 22-α (SM22α) genes, well defined VSMC markers (Figure 2D and 2E), while β-actin protein levels were decreased. Such a decrease in β-actin protein levels is probably due to the suppression of mTOR activity (see below) because the AMPK/mTOR pathway is known to regulate the expression of the genes relevant to

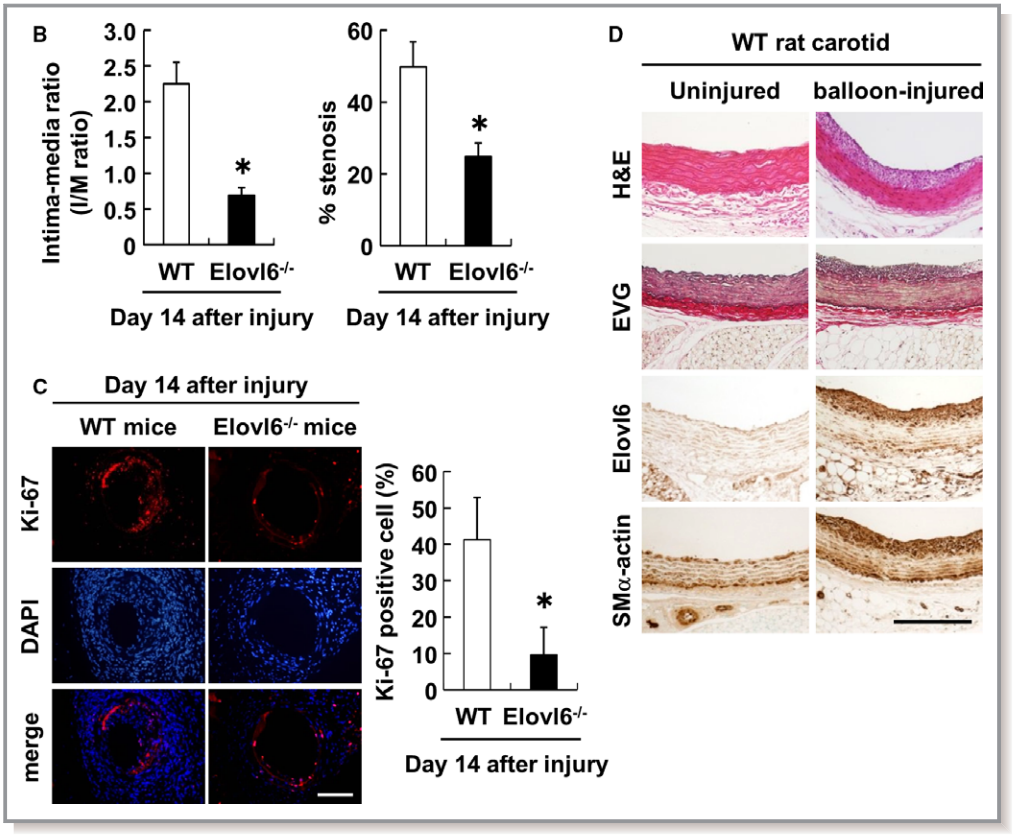

Figure 1. continued

cellular proliferation.[22] In contrast, the adenovirus-mediated overexpression of Elovl6 increased the expression of these genes (Figure S4A and S4B) in HASMC, suggesting that Elovl6-driven fatty acid metabolism plays an important role in the regulation of VSMC differentiation.

Elovl6 Regulates Cell Cycle Inhibitory Gene and Protein Expression

To determine the mechanisms by which Elovl6 knockdown reduces VSMC proliferation, we examined the expression of mRNAs and proteins critical for cell proliferation in HASMC transfected with either siElovl6 or siGFP. The results obtained showed that knockdown of Elovl6 increased the p53 expression by 1.2-fold and p21 expression by 2.0-fold and decreased the mRNA levels of mammalian target of rapamycin (mTOR), a serine/threonine protein kinase that phosphorylates the binding protein essential for translational initiation and protein synthesis, by 45% (Figure 3A). Consistent with these results, the mRNA levels of p53 and p21 in the aorta were 1.3- and 2.9-fold higher, respectively, while those of mTOR were comparable between Elovl6$^{-/-}$ and WT mouse aorta (Figure 3A). Knockdown of Elovl6 induced the phosphorylation of p53 tumor suppressor and protein expression of cyclin-dependent kinase inhibitor p21 (Figure 3B). An increase in the expression of p21 is likely due to the activation of p53 given that the p21 gene is a direct target of p53.[23] The phosphorylation of mTOR was clearly decreased in siElovl6-transfected HASMC (Figure 3B).

Conversely, the overexpression of Elovl6 increased mTOR mRNA levels (Figure S4C). To further analyze the role of p21 in HASMC with silenced Elovl6, siRNA for p21 was transfected with or without siRNA for Elovl6, and the effects of the silencing of p21 on thymidine uptake were evaluated. The p21 siRNA treatment resulted in an increase in the uptake of thymidine, and, more importantly, the repressed thymidine uptake in cells with Elovl6 knockdown was completely reversed by p21 siRNA treatment (Figure 3C). These results indicate that the Elovl6 knockdown reduces cell proliferation largely through the induction of p21 expression.

Elovl6 Deficiency Induces AMPK Activity in VSMC

AMP-activated protein kinase (AMPK), a heterotrimeric serine/threonine protein kinase that is primarily activated in response to nutrients and energetic stress,[24-26] has been shown to regulate cell proliferation via a p53 and p21 pathway in response to vascular injury.[27,28] To explore the effects of Elovl6 deficiency on AMPK activation, we performed Western blot analysis by using the antibody against phosphopeptides

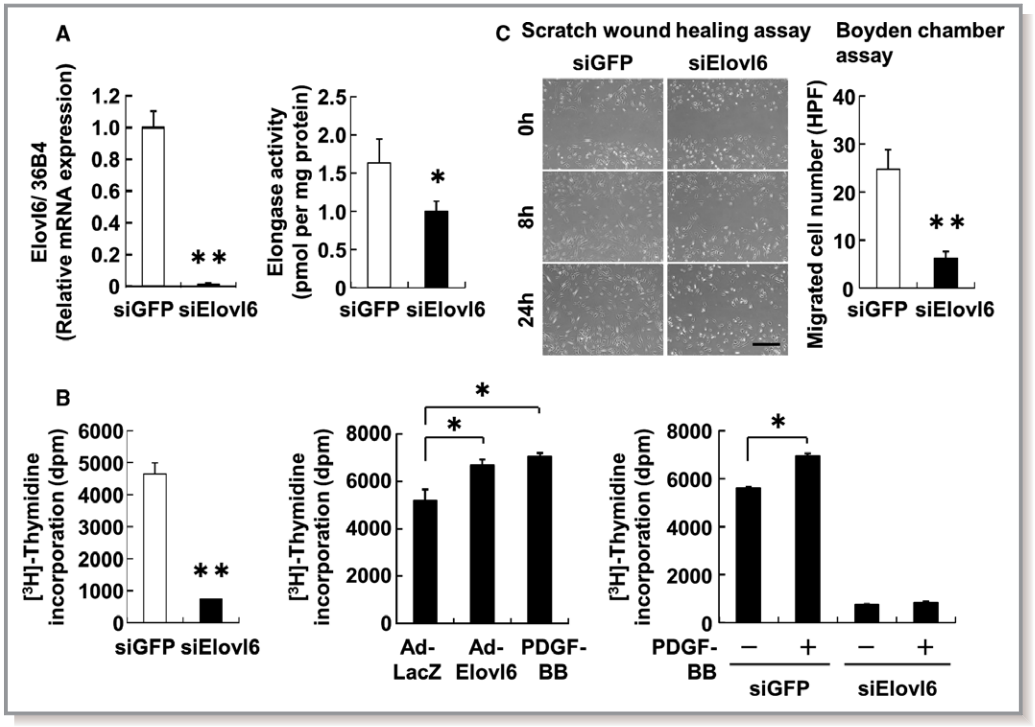

Figure 2. Inhibition of Elovl6 gene expression suppresses VSMC proliferation and migration. A, qRT-PCR for Elovl6 mRNA expression and Elovl6 enzymatic activity in HASMC transfected with Elovl6 (n=6) or GFP siRNA (n=6). Elovl6 siRNA suppressed Elovl6 mRNA expression and activity more strongly than GFP siRNA. Specific activity was expressed as picomoles of radioactive [2-^{14}C]malonyl-CoA incorporated into hydrophobic long-chain fatty acid fractions by 1 mg of microsomal protein. B, The [^{3}H]thymidine uptake assay in HASMC transfected with Elovl6 (n=6) or GFP siRNA (n=6), or adenovirus-mediated overexpression of Elovl6 (n=6) or LacZ (n=6). The knockdown of Elovl6 expression markedly suppressed the incorporation of [^{3}H]thymidine, whereas its overexpression induced the uptake of [^{3}H]thymidine significantly more than the PDGF-BB treatment (10 ng/mL, n=6) for 24 hours. The PDGF-BB-induced incorporation of [^{3}H]thymidine was canceled by the siRNA-mediated knockdown of Elovl6. C, Scratch assay and Boyden chamber assay in HASMC transfected with Elovl6 (n=6) or GFP siRNA (n=7). The knockdown of Elovl6 markedly suppressed cell migration. The number of migrated cells was counted under a light microscope. Scale bar=200 μm. D and E, qRT-PCR for SMα-actin and SM22α mRNA expression (D) and Western blot for protein expression (E) in HASMC transfected with Elovl6 (n=6) or GFP siRNA (n=6) and in the aorta of Elovl6$^{-/-}$ mice (n=6) or WT mice (n=6). The mRNA levels of SMα-actin and SM22α assessed by qRT-PCR, normalized by mRNA levels of the nuclear single-copy housekeeping gene 36B4, were significantly decreased by siRNA-mediated knockdown of Elovl6 or in Elovl6$^{-/-}$ mouse aorta. The levels of protein expression for SMα-actin and SM22α were normalized by β-actin. Each experiment was performed at least 3 times. All values are represented as the means±SEM of 3 experiments. *P<0.05, **P<0.01, as measured by the Mann-Whitney U-test, Student t test, or Tukey-Kramer test. Elovl6 indicates elongation of long-chain fatty acid family member 6; HASMC, human aortic smooth muscle cells; PDGF-BB, platelet-derived growth factor-BB; SMα-actin, smooth muscle α-actin; SM22α, smooth muscle protein 22α; WT, wild-type C57BL/6 mice.

containing Thr-172 of the α subunit of human AMPK. Results showed that knockdown of Elovl6 markedly induced the phosphorylation of AMPK in HASMC and that the total protein levels of AMPK were comparable between siGFP- and siElovl6-transfected cells. The p21 protein levels were increased while β-actin protein levels were decreased (Figure 3B). Consistently, Elovl6$^{-/-}$ mice exhibited significantly increased phosphorylated AMPK levels and slightly decreased β-actin levels compared to WT mice (Figure 3D). In contrast, the overexpression of Elovl6 decreased phosphorylation of AMPK (Figure S4D).

AMPK activation has been shown to mediate an increase in fatty acid oxidation via acetyl-CoA carboxylase (ACC) phosphorylation at Ser-78, which leads to inactivation of ACC activity and reduction of malonyl-CoA synthesis, in the setting of metabolic stress.[29] We found that ACC phosphorylation is associated with AMPK activation in HASMC with Elovl6 knockdown (Figure 3B), providing evidence that AMPK activity

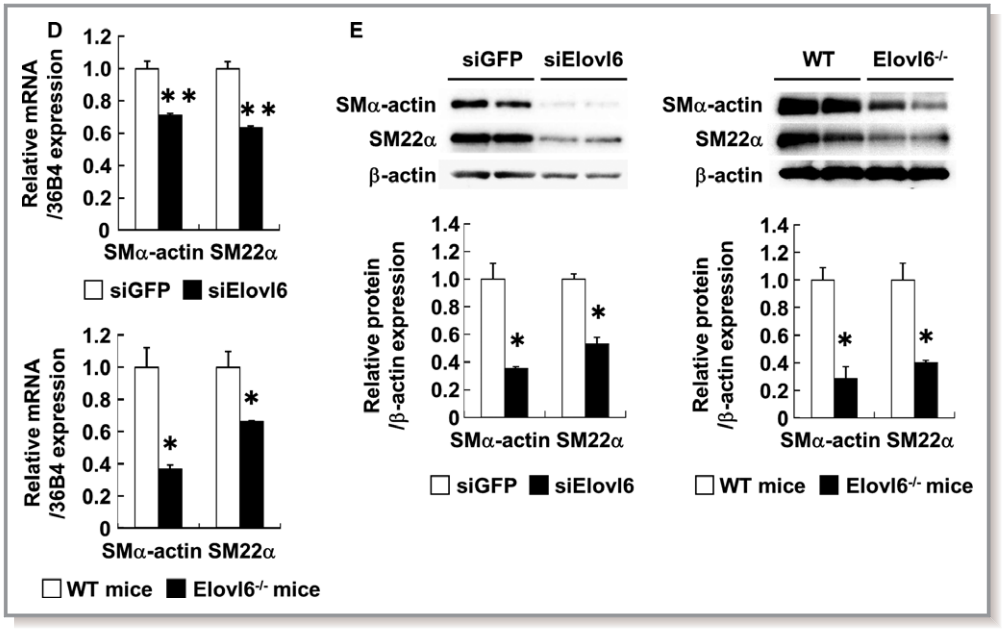

Figure 2. continued

is indeed increased in these cells. Because inhibition of ACC and subsequent decrease in malonyl-CoA production lead to a suppression of lipogenesis and favor fatty acid oxidation through an induction of carnityl palmitoyltransferase (CPT) shuttle system,[30] it is likely that Elovl6-deficient VSMC has reduced synthesis and increased oxidation of LCFA. As expected, FA oxidation rate, as assessed by using [^{14}C]-palmitic acid, was higher in VSMC transfected with siElovl6 in comparison with siGFP-transfected VSMC. Furthermore, the mRNA levels of peroxisome proliferator-activated receptor (PPAR)α, the nuclear receptor playing a crucial role as an activator of genes involved in fatty acid oxidation,[31] were increased in HASMC with Elovl6 knockdown as compared with siGFP-transfected cells (data not shown).

Elovl6 Knockdown Alters LCFA Composition in VSMC In Vivo and In Vitro

To determine the effect of Elovl6 knockdown on LCFA metabolism, we examined the composition of LCFA in lipids extracted from the aorta of Elovl6$^{-/-}$ and WT mice. Saturated palmitate (C16:0) levels were higher, and monounsaturated oleate (C18:1 n-9) levels were lower in Elovl6$^{-/-}$ mice than in WT mice (Figure 4A). The qRT-PCR revealed that the aortic expression of the gene for SCD1, a rate-limiting enzyme that converts saturated fatty acids (SFAs) to monounsaturated fatty acids, was lower in Elovl6$^{-/-}$ mice than in WT mice (Figure 4B) (60% of the control value, $P<0.05$).

Alterations of the composition of LCFA and reductions of the expression of SCD1 in the aorta of Elovl6$^{-/-}$ mice were recapitulated by Elovl6 siRNA treatment in vitro (Figure 4C and 4D). These results also indicate that metabolic phenotype such as a lower oleate (C18:1 n-9) levels with an Elovl6 knockdown may be partially due to a decrease in SCD1 activity. In contrast, the overexpression of Elovl6 in HASMC decreased palmitate and palmitoleate (C16:1 n-7) levels and increased oleate levels (Figure S5A), whereas the mRNA levels of SCD1 were similar in HASMC transduced with Ad-Elovl6 or Ad-LacZ (Figure S5B). Taken together, these results indicate that Elovl6 in VSMC plays a major role in determining the fatty acid composition of LCFA in VSMC.

Effects of Palmitate and Oleate on Cell Proliferation and Cell Cycle Regulators

Given the data presented above, we examined the effects of palmitate and oleate on VSMC proliferation and cell cycle regulatory gene expression. Palmitate treatment reduced the incorporation of [^{3}H]thymidine by 30% ($P<0.05$), whereas oleate treatment increased it by 20% ($P<0.01$) (Figure 5A). The qRT-PCR analysis also revealed that palmitate suppressed the SMα-actin (72%, $P<0.05$), SM22α (56%, $P<0.05$), p53 (1.4-fold, $P<0.01$), and p21 (1.8-fold, $P<0.01$) mRNA levels, whereas oleate increased the mTOR mRNA levels (1.6-fold, $P<0.01$) (Figure 5B). Western blot analysis also showed that palmitate treatment decreased protein levels of SMα-actin and SM22α (Figure 5C). Furthermore, palmitate treatment significantly induced the phosphorylation of AMPK, ACC, and p53, increased the expression of p21, and decreased the phosphorylation of mTOR (Figure 5D). In contrast, oleate

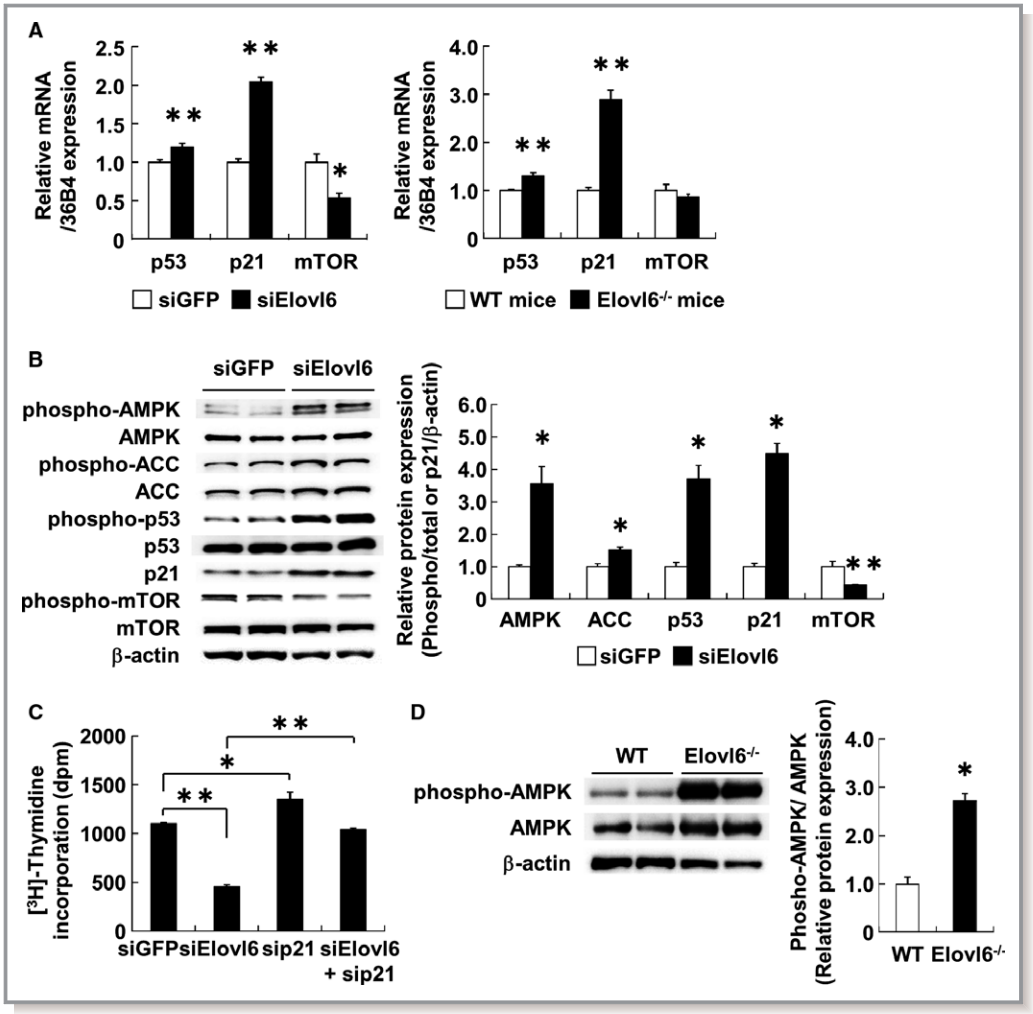

Figure 3. Depletion of Elovl6 expression modulates cell cycle regulators in HASMC. A, qRT-PCR for p53, p21, and mTOR mRNA expression in HASMC transfected with Elovl6 (n=6) or GFP siRNA (n=8) and in the aorta of Elovl6$^{-/-}$ mice (n=6) or WT mice (n=6). The expression levels of p53 and p21 mRNA, normalized by mRNA levels of 36B4, were significantly induced while that of mTOR mRNA was significantly decreased by siRNA-mediated knockdown of Elovl6 or in the Elovl6$^{-/-}$ mice aorta. B, Western blot analysis of each protein level involved in cell proliferation in HASMC. Protein levels were normalized by β-actin. The knockdown of Elovl6 (n=5) significantly induced the phosphorylation of AMPK, ACC, and p53 and expression of p21 but reduced the phosphorylation of mTOR more than that in the siGFP-transfected control cells (n=7). C, Effects of p21 gene silencing on the antiproliferative effects of the knockdown of Elovl6 in HASMC. Elovl6 siRNA-mediated antiproliferative effects were canceled by p21 depletion (siGFP, siElovl6, sip21: n=6; siElovl6+sip21: n=5). D, Western blot analysis of the aorta of Elovl6$^{-/-}$ mice (n=6) or WT mice (n=6). The phosphorylation of AMPK in the aorta was markedly increased in Elovl6$^{-/-}$ mice compared to WT mice. Western blot data for phosphorylation of proteins were normalized by total proteins in the same samples and expressed as a fold increase from the mean level of siGFP or the WT mice. Each experiment was performed at least 3 times. All values are represented as the means±SEM of 3 experiments. **P*<0.05, ***P*<0.01, as measured by the Mann-Whitney U-test (A, B, and D) or the Tukey-Kramer test (C). ACC indicates acetyl-CoA carboxylase; AMPK, AMP-activated protein kinase; Elovl6, elongation of long-chain fatty acid family member 6; HASMC, human aortic smooth muscle cells; mTOR, mammalian target of rapamycin; WT, wild-type C57BL/6 mice.

treatment decreased total protein levels of AMPK, ACC, and p53 and p21, and increased total mTOR levels, as previously reported,[32-35] and as such, levels of phosphorylated form of AMPK, ACC, and p53 were decreased, and levels of phosphorylated form of mTOR were increased (Figure 5D). A simultaneous stimulation with palmitate and oleate consistently showed that each of these 2 LCFAs antagonizes the effects of the other (Figure 5A through 5D).

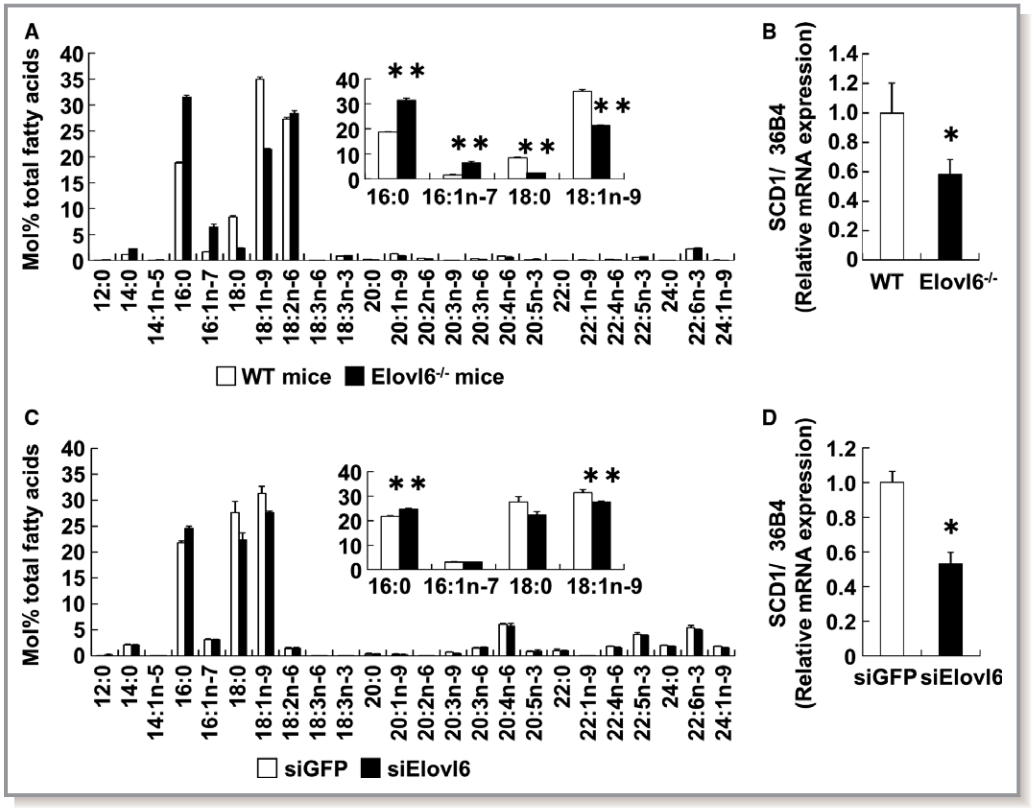

Figure 4. Elovl6 depletion modulates fatty acid composition in vivo and in vitro. A and B, Fatty acid composition of a lipid extract (A) and qRT-PCR for SCD1 gene expression (B) from the aorta of Elovl6$^{-/-}$ (n=5) or WT mice (n=4). The relative amounts of palmitate (C16:0) were higher, whereas those of oleate (C18:1 n-9) were lower in Elovl6$^{-/-}$ mice than in WT mice (A). SCD1 mRNA levels, normalized by mRNA levels of 36B4, were lower in Elovl6$^{-/-}$ mice (n=5) than in WT mice (n=4) (B). C and D, Fatty acid composition of a neutral lipid extract (C) and qRT-PCR for SCD1 gene expression (D) in HASMC transfected with Elovl6 (n=5) or GFP siRNA (n=6). Along with in vivo data, the relative amounts of palmitate were significantly higher, whereas those of oleate (C) and SCD1 mRNA levels, normalized by mRNA levels of 36B4 (D), were lower with the knockdown of Elovl6 than with siGFP transfection. mRNAs of the WT mice (B) and siGFP (D) control group were normalized to a value of 1, and mRNA levels in Elovl6$^{-/-}$ mice or Elovl6 siRNA cells are shown relative to the control level. Each experiment was performed at least 3 times. All values are represented as the means±SEM of 3 experiments. *P<0.05, **P<0.01, as measured by the Mann-Whitney U-test. Elovl6 indicates elongation of long-chain fatty acid family member 6; HASMC, human aortic smooth muscle cells; SCD1, stearoyl-CoA desaturase 1; WT, wild-type C57BL/6 mice.

Elovl6 Knockdown Induces KLF4 Expression in VSMC

Krüppel-like factor 4 (KLF4), a reprogramming factor that promotes induced pluripotent stem (iPS) cell formation,[36] controls the expression of VSMC marker genes.[37,38] KLF4 induces the expression of p21 in concert with the activation of p53 and as a result decreases the proliferation of VSMC.[38] We performed a series of experiments to test whether KLF4 is involved in the suppression of proliferation of Elovl6 siRNA-transfected HASMC. Immunohistochemistry revealed that KLF4 expression was more evident in Elovl6$^{-/-}$ mice than in WT mice in both uninjured and wire-injured aorta (Figure 6A). Western blot and qRT-PCR analyses using protein and RNA extracts from aorta, respectively, confirmed these findings (Figure 6B). In addition, Elovl6 knockdown led to a robust elevation in KLF4 expression at both protein and mRNA levels (Figure S6A and S6B). Overexpression of Elovl6 suppressed the KLF4 protein and mRNA levels (Figure S6C and S6D), substantiating the above findings. Of note, exogenous palmitate significantly upregulated KLF4 protein and mRNA levels, and oleate blunted these effects (Figure 6C and Figure S6E), further supporting the findings that KLF4 expression is regulated by Elovl6-driven fatty acid metabolism.

KLF4 Knockdown Mitigates Upregulation of p53 and p21 in Elovl6-Deficient VSMC

We next examined the cell cycle regulatory gene expression and cell proliferation in HASMC with Elovl6 knockdown.

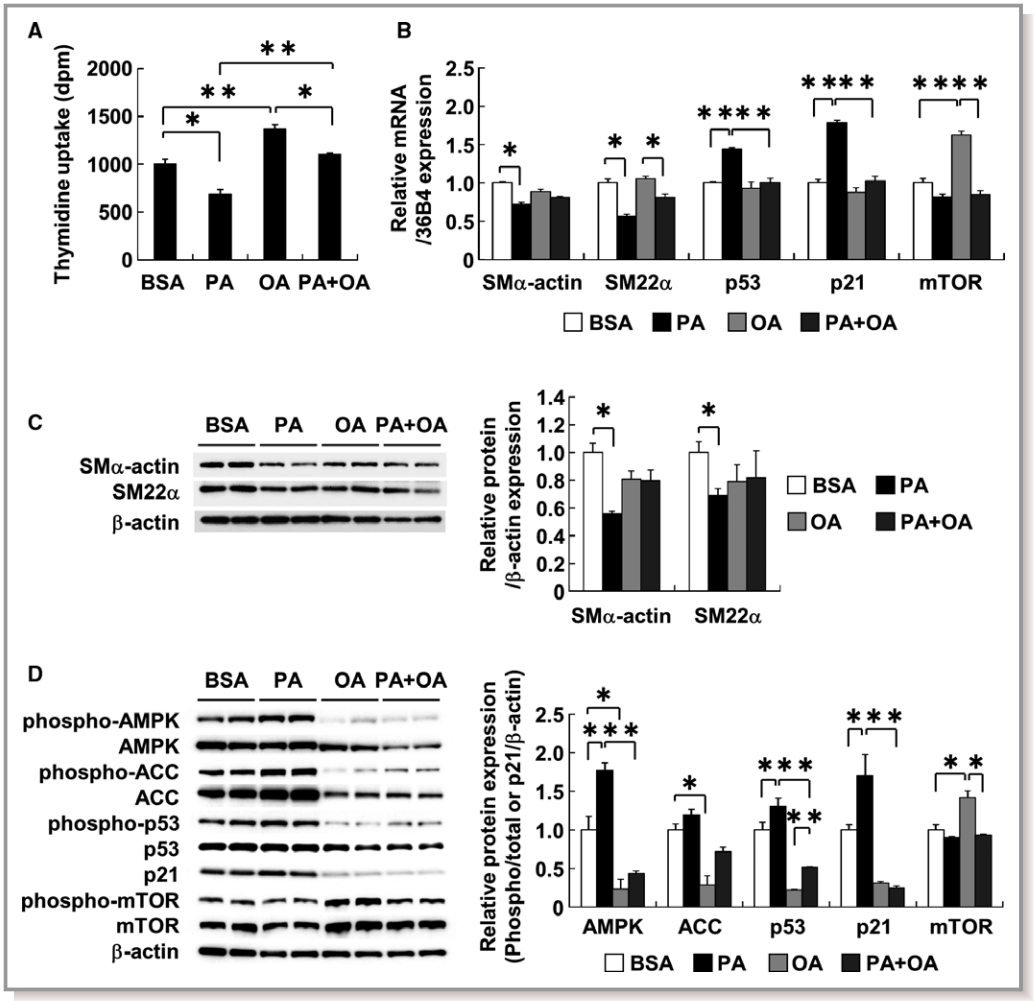

Figure 5. Palmitate suppresses cell proliferation by altering cell cycle regulatory proteins in HASMC. A, [^{3}H]Thymidine uptake assay in HASMC treated with PA or OA. PA (250 μmol/L) treatment significantly suppressed, whereas OA (250 μmol/L) treatment induced, the incorporation of [^{3}H]thymidine (BSA, OA: n=6; PA: n=8). Simultaneous treatment with OA significantly inhibited PA-induced antiproliferative effects (PA+OA: n=6). B, qRT-PCR for SMα-actin, SM22α, p53, p21, and mTOR mRNA levels, normalized by mRNA levels of 36B4, in HASMC treated with PA or OA (BSA: n=7; PA, OA, PA+OA: n=6). The mRNA levels for SMα-actin and SM22α were significantly decreased, whereas that of p21 and p53 mRNA levels were increased by PA treatment. In contrast, mTOR mRNA levels were significantly increased by OA treatment. mRNA levels in the siGFP control group were normalized to a value of 1, and those in cells treated with various stimuli are shown relative to the control level. C and D, Western blot analysis of each protein level involved in cell proliferation in HASMC treated with PA or OA (BSA: n=8; PA, OA, PA+OA: n=6). PA markedly induced the phosphorylation of AMPK, ACC, and p53 and expression of p21, whereas OA induced the phosphorylation of mTOR. Simultaneous treatment with PA and OA mutually suppressed the induction of protein expression. Furthermore, treatment of PA decreased SMα-actin and SM22α protein expression. Western blot data for phosphorylation of proteins were normalized by total protein amount in the same samples and expressed as a fold increase from the mean level of the BSA group; p21 protein levels were normalized by β-actin protein levels. Each experiment was performed at least 3 times. All values are represented as the means±SEM of 3 experiments. *P<0.05, **P<0.01, as measured by the Tukey-Kramer test (A and B) or the Steel-Dwass test (C and D). ACC indicates acetyl-CoA carboxylase; AMPK, AMP-activated protein kinase; BSA, fatty acid-free bovine serum albumin; HASMC, human aortic smooth muscle cells; mTOR, mammalian target of rapamycin; OA, oleic acid; PA, palmitic acid; SM22α, smooth muscle protein 22α; SMα-actin, smooth muscle α-actin.

After confirming substantial depletion of KLF4 (Figure S7A and S7B), we performed qRT-PCR analysis. Simultaneous knockdown of KLF4 partly rescued the suppressed proliferation in siElovl6-transfected HASMC (Figure S7C). Consistent with these results, knockdown of KLF4 abrogated the increase in phospho-p53 and p21 protein levels

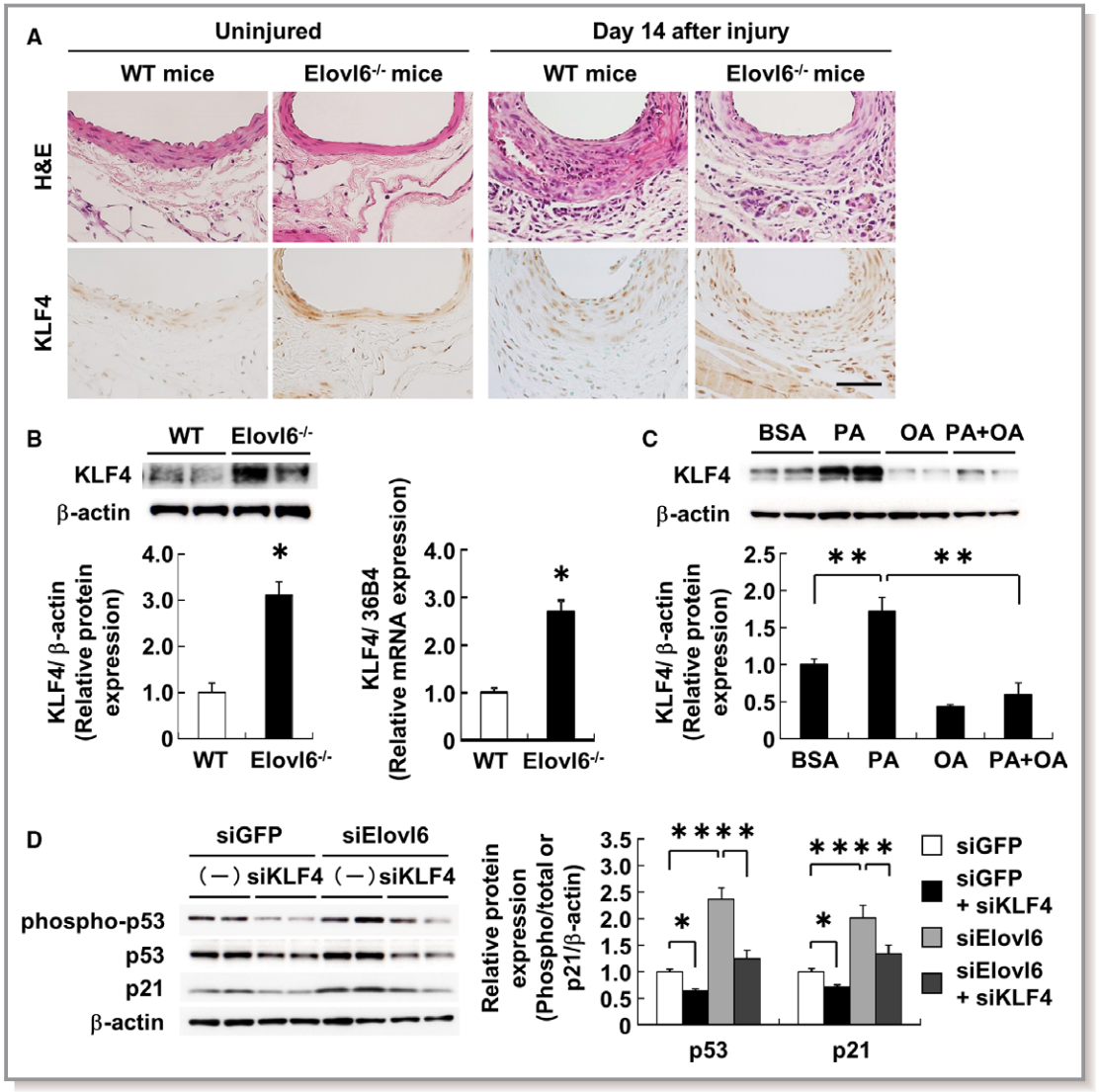

Figure 6. Elovl6 deficiency directly induces KLF4 expression through AMPK activation. A, Immunohistochemical staining with an anti-KLF4 antibody in femoral artery sections from Elovl6$^{-/-}$ or WT mice. Expression of KLF4 was significantly increased in the medial layer of the aorta of Elovl6$^{-/-}$ mice compared to WT mice before or after wire injury. Scale bar=200 μm. B, Western blot and qRT-PCR analyses of KLF4 expression in the aorta of Elovl6$^{-/-}$ mice (n=6). KLF4 expression was significantly induced in the Elovl6$^{-/-}$ mice aorta compared to WT mice (n=6). C, Western blot analysis of KLF4 in HASMC treated with PA or OA. KLF4 was significantly increased by PA treatment but decreased by OA treatment (BSA, PA: n=8; OA, PA+OA: n=6). D, Effects of KLF4 gene silencing on Elovl6 siRNA-induced cell cycle regulatory proteins in HASMC by Western blot analysis. Elovl6 siRNA-induced phospho-p53 or p21 protein levels were suppressed by the depletion of KLF4 (siGFP, siElovl6, siGFP, or siElovl6+siKLF4: n=6). E, Western blot analysis of AICAR (1 mmol/L, n=6) and Compound C (10 μmol/L, n=6) stimulations in HASMC. Treatment of AICAR induced the KLF4 expression in a time-dependent manner, but costimulation with Compound C (n=6) reduced the AICAR-induced expression of KLF4. F, Western blot analysis of KLF4 in GFP siRNA (n=5)- or Elovl6-siRNA (n=6)-transfected HASMC with or without Compound C. Compound C abrogated the Elovl6 siRNA-induced expression of KLF4. The mRNA levels determined by qRT-PCR were normalized by 36B4, and protein levels determined by Western blot analysis were normalized by β-actin levels. Each experiment was performed at least 3 times. All values are represented as the means±SEM of 3 experiments. *P<0.05, **P<0.01, as measured by the Mann-Whitney U-test (B), or the Steel-Dwass test (C through F). AICAR indicates 5-aminoimidazole-4-carboxamide ribonucleotide; BSA, fatty acid-free bovine serum albumin; Elovl6, elongation of long-chain fatty acid family member 6; H&E, hematoxylin-eosin; HASMC, human aortic smooth muscle cells; KLF4, Krüppel-like factor 4; OA, oleic acid; PA, palmitic acid; WT, wild-type C57BL/6 mice.

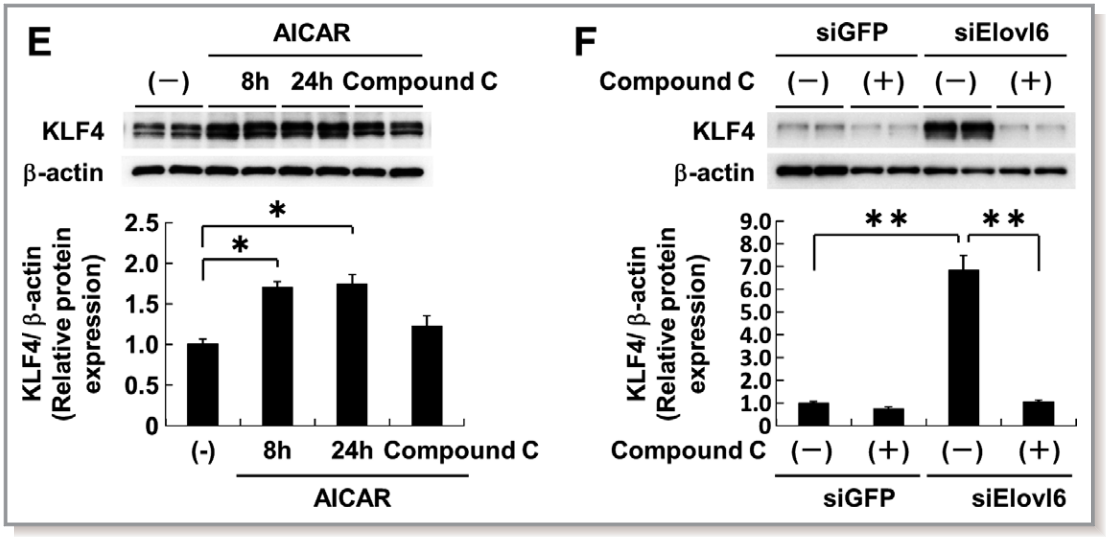

Figure 6. continued

as well as p53 and p21 mRNA levels observed in HASMC with Elovl6 knockdown (Figure 6D and Figure S7D). These results suggest that KLF4 mediates in part an induction of p21 and p53 expression observed in HASMC with Elovl6 deficiency.

KLF4 Knockdown Affects SMC Marker Gene Expression in a Context-Dependent Manner

KLF4 has been shown to act as potent repressor of VSMC gene transcription in cultured VSMCs through multiple mechanisms including the repression of function and expression of muscle-restricted transcription coactivator myocardin.[38-40] Thus, it is anticipated that KLF knockdown enhances VSMC marker gene expression. Unexpectedly, however, we found that mRNA expression of SMα-actin and SM22α was significantly reduced in HASMC with KLF4 knockdown (Figure S8A). Nevertheless, Western blot analysis revealed that the protein levels of SMα-actin and SM22α were not changed in HASMC transfected with siKLF4 (Figure S8B). The most likely explanation for these apparently contradictory results would be that experimental conditions may affect the role of KLF4 on SMC gene expression, given that KLF4 only transiently binds to the SMC promoters at an early time point after KLF4 induction.[38] Indeed, we found that siRNA-mediated Elovl6 or KLF4 knockdown increased SMα-actin or SM22α expressions at an early time point (8-24 hours after transfection of siRNA); however, Elovl6 or KLF4 knockdown markedly suppressed SMC marker gene expression 48 hours after transfection (Figure S8C).

AMPK Directly Activates KLF4 Expression in VSMC In Vitro

To determine whether AMPK activates KLF4 expression, we examined the effects of a pharmacological AMPK activator (5-aminoimidazole-4-carboxamide ribonucleotide; AICAR) or inhibitor (Compound C) on KLF4 protein expression. AICAR significantly induced KLF4 protein levels in a time-dependent manner, and Compound C diminished this effect (Figure 6E). Of importance, Compound C completely abrogated an increase in KLF4 protein levels observed in HASMC with Elovl6 knockdown (Figure 6F). In contrast, KLF4 knockdown had no effects on phosphorylation of AMPK (Figure S9). Taken together, these results identify KLF4 as a bona fide direct target of AMPK.

AMPK Phosphorylation Is Induced by Oxidative Stress

To explore the mechanisms by which Elovl6 deficiency leads to an induction of AMPK phosphorylation in VSMC, we examined the reactive oxygen species (ROS) production in Elovl6$^{-/-}$ mice. Immunohistochemistry revealed that nitrotyrosine immunoreactivity, used as a marker of oxidative stress, was fairly detectable in Elovl6$^{-/-}$ mice but poorly detectable in WT mice (Figure 7A). At 14 days after wire injury, however, nitrotyrosine immunoreactvity was clearly enhanced in both WT and Elovl6$^{-/-}$ mice (Figure 7A). Furthermore, we found that siRNA knockdown of Elovl6 induced ROS production as assessed by using CM-H_2DCFDA probe in HASMC (Figure 7B). In addition, palmitate induced ROS production, and oleate inhibited this palmitate-induced ROS production in HASMC (Figure 7B). Quantitation using a fluorometric assay, which primarily detects production of H_2O_2, showed that Elovl6 knockdown and exposure to palmitate increased production of H_2O_2 in HASMC by 1.7- and 1.9-fold, respectively, compared with controls (Figure 7C). To explore whether mitochondria could be involved in ROS production, we measured mitochondria-derived superoxide levels by using mitoSOX fluorescent probes (Life Technologies, Carlsbad, CA). However, we could hardly detect the difference in signal

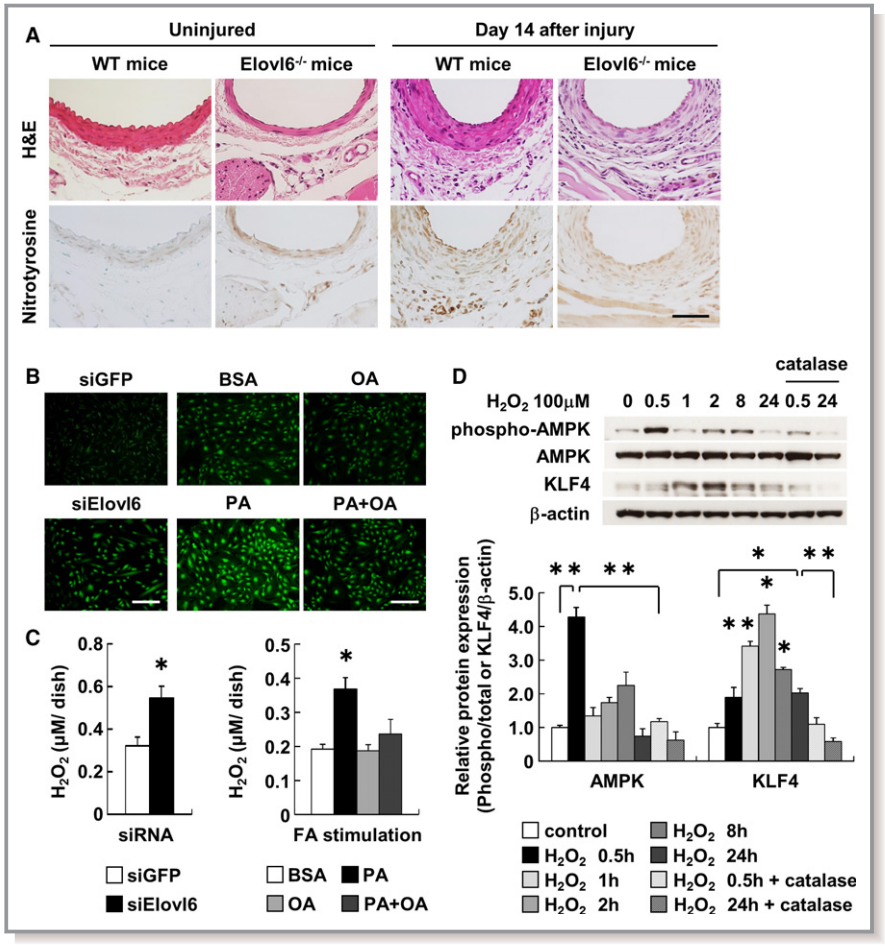

Figure 7. ROS generation induces phosphorylation of AMPK and KLF4 expression in VSMC. A, Immunohistochemical staining with an antibody against nitrotyrosine in femoral artery sections from Elovl6$^{-/-}$ or WT mice. The nitrotyrosine-positive cells were significantly increased in the medial layer of the aorta of Elovl6$^{-/-}$ mice compared to WT mice before or after wire injury. Scale bar=200 μm. B, Intracellular ROS production was detected using oxidant-sensitive fluorogenic probe CM-H_2DCFDA in HASMC. The siRNA-mediated Elovl6 knockdown or stimulation with PA (250 μmol/L) increased ROS levels in comparison with siGFP or BSA. Costimulation of OA (250 μmol/L) significantly reduced PA-induced ROS generation. Scale bar=200 μm. C, fluorometric assay showed increased H_2O_2 generation in HASMC transfected with Elovl6 siRNA (siGFP, siElovl6: n=6) or treated with PA (BSA, PA, OA, PA+OA: n=6). D, Western blot analysis of AMPK and KLF4 in HASMC treated with 100 μmol/L H_2O_2. Phosphorylation of AMPK was normalized by total AMPK protein amount, and KLF4 protein levels were normalized by β-actin levels. Relative protein expression was expressed as a fold increase from the mean level of the controls. Exposure to H_2O_2 (n=3 per group) significantly induced phosphorylation of AMPK and KLF4 expression. Costimulation with catalase (1 unit, n=3 per group) significantly reduced H_2O_2 induction of these expressions. E, qRT-PCR for KLF4, SMα-actin, and SM22α mRNA levels in HASMC treated with 100 μmol/L H_2O_2 for 24 hours (control: n=6; H_2O_2: n=8). KLF4 mRNA levels, normalized by mRNA levels of 36B4, were significantly increased, whereas SMα-actin and SM22α mRNA levels were decreased by H_2O_2 treatment. F, Western blot analysis also showed that exposure of HASMC to H_2O_2 decreased protein expression of SMα-actin and SM22α, normalized by β-actin levels (control, H_2O_2: n=6). Each experiment was performed at least 3 times. All values are represented as the means±SEM of 3 experiments. *P<0.05, **P<0.01, as measured by the Tukey-Kramer test (C), Steel-Dwass test (D), or Mann-Whitney U-test (E and F). AMPK indicates AMP-activated protein kinase; BSA, fatty acid-free bovine serum albumin; CM-H_2DCFDA, 5-(6)-chloromethyl-2′, 7′-dichlorodihydrofluorescein diacetate acetyl ester; Elovl6, elongation of long-chain fatty acid family member 6; H&E, hematoxylin-eosin; H_2O_2, hydrogen peroxide; HASMC, human aortic smooth muscle cells; KLF4, Krüppel-like factor 4; OA, oleic acid; PA, palmitic acid; ROS, reactive oxygen species; SM22α, smooth muscle protein 22α; SMα-actin, smooth muscle α-actin; WT, wild-type C57BL/6 mice.

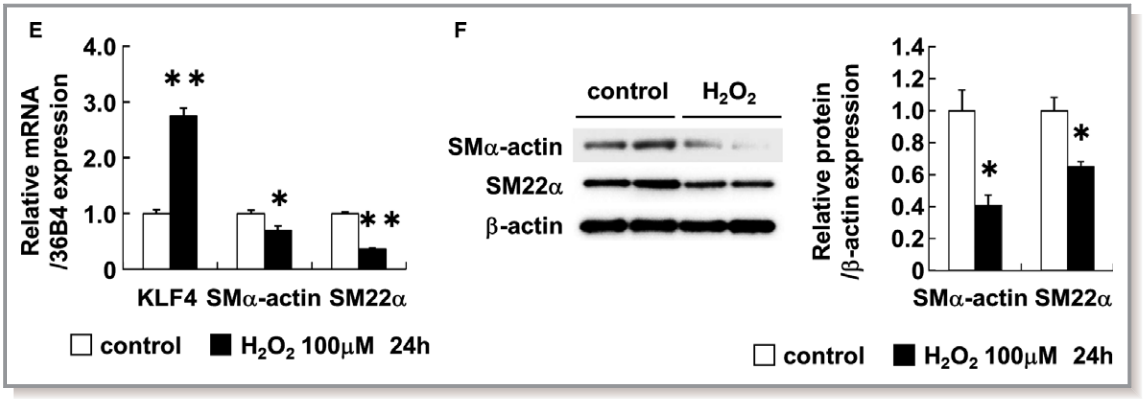

Figure 7. continued.

intensity among siElovl6-transfected HASMC, palmitate-treated HASMC, and control cells, suggesting that excessive superoxide is not likely to be generated in mitochondria in either siElovl6-transfected or palmitate-treated HASMC.

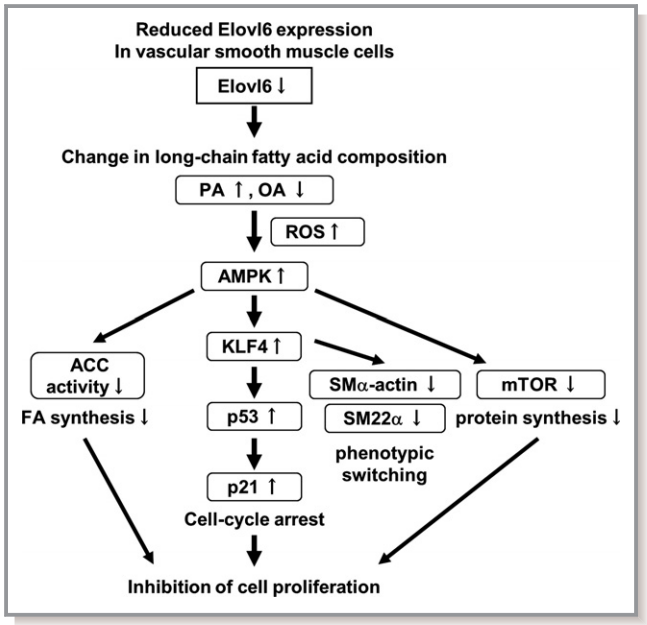

Figure 8. Schematic diagram of the molecular mechanisms for phenotypic modulation of VSMC in Elovl6-deficient VSMC. A reduction in the expression of Elovl6 in VSMC induces change in the fatty acid composition; C16 PA is increased, and C18 OA is decreased, in vivo and in vitro. These changes in FA composition induce ROS production that leads to AMPK activation, an increase in KLF4, p53, and p21 expression, decreases in SMα-actin, SM22α, and mTOR expression, and a decrease in ACC activity. Thus, Elovl6-mediated derangement of FA composition in VSMC induces phenotypic switching of VSMC. ACC indicates acetyl-CoA carboxylase; AMPK, AMP-activated protein kinase; Elovl6, elongation of long-chain fatty acid family member 6; FA, fatty acid; KLF4, Krüppel-like factor 4; mTOR, mammalian target of rapamycin; OA, oleic acid; PA, palmitic acid; ROS, reactive oxygen species; SM22α, smooth muscle protein 22α; SMα-actin, smooth muscle α-actin; VSMC, vascular smooth muscle cells.

We found that exposure of HASMC to hydrogen peroxide (H_2O_2 100 μmol/L) resulted in induced AMPK phosphorylation and subsequently increased KLF4 expression (Figure 7D). Catalase, an antioxidant that eliminates H_2O_2, prevented H_2O_2-induced AMPK phosphorylation and KLF4 expression in HASMC (Figure 7D). Furthermore, exposure of HASMC to H_2O_2 increased KLF4 mRNA and decreased SMα-actin and SM22α mRNA levels (Figure 7E). Western blot analysis also showed that exposure of HASMC to H_2O_2 decreased protein levels of SMα-actin and SM22α (Figure 7F). These results suggest that ROS is an important mediator for the induction of AMPK phosphorylation and the resulting KLF4 expression in Elovl6-deficient VSMC.

Discussion

In the present study we examined the role of Elovl6-mediated LCFA metabolism in the regulation of VSMC phenotypic switching in vivo and in vitro. To summarize, results shown here are depicted in Figure 8. Elovl6 deficiency causes an increase in intracellular palmitate and a decrease in oleate, both of which contribute to ROS production and promote phosphorylation and activation of AMPK. As a consequence of AMPK activation, KLF4 is induced to increase p53 and p21 expression, ACC is phosphorylated, and mTOR is dephosphorylated. Our findings strongly indicate the pivotal role of Elovl6-driven fatty acid metabolism in the regulation of proliferation and differentiation of VSMC, 2 pathophysiological processes that determine VSMC phenotype.

One of the seminal findings in this study is that KLF4 expression is robustly induced in Elovl6$^{-/-}$ mouse aorta and VSMC with siRNA knockdown of Elovl6. Elovl6 siRNA-transfected VSMC is characterized by reduced proliferation and migration as well as reduced expression of VSMC markers. More importantly, these changes are likely to be at least partly ascribed to KLF4 induction because KLF4 knockdown mitigates activation of the cell cycle inhibitory

genes p53 and p21 in Elovl6-deficient VSMC. These results are consistent with the previous reports demonstrating that KLF4 induces cell cycle arrest.[38,41-44]

Of note, induction of KLF4 expression by Elovl6 knockdown is dependent on AMPK activation, based on the results that Compound C, a specific inhibitor of AMPK, completely abrogated KLF4 induction. Our data also indicate that KLF4 is required for AMPK-induced p21 expression. Collectively, our results demonstrate that KLF4 is one of the primary genes that regulate cellular response to AMPK activation.

It is notable that VSMC transfected with siElovl6 displays downregulation of SMC marker gene expression along with decreased proliferation and migration activities, given that the loss of SMC marker gene expression is generally coupled with the increased proliferation and migration during phenotypic transition.[2] Our findings that the AMPK/KLF4 axis plays a central role in phenotypic transition in VSMC with Elovl6 knockdown prompt us to speculate that the phenotype of Elovl6-deficient VSMC may be relevant to cellular senescence-associated phenotype. Cellular senescence is observed in most mammalian cells in the setting of a variety of stresses including alterations in intracellular metabolism.[45] Emerging evidence indicates that AMPK activation and resulting p53-p21 axis activation promote senescent phenotype, the hallmarks of which are the irreversible loss of proliferative potential and acquisition of altered differentiated function.[46] We found that Elovl6 knockdown induces apoptosis as assessed by the activation of caspase 3/7 to some extent (data not shown), suggesting that altered Elovl6-mediated LCFA metabolism induces both apoptosis and perhaps a state of senescence. Further work will be warranted to define such previously unrecognized phenotypes.

A recent SMC lineage-tracing study demonstrates that substantial numbers of macrophage-like cells within the atherosclerotic plaques are derived from VSMC in apolipoprotein E (apoE)-knockout mice and in humans.[8] In addition, VSMC-specific conditional knockout of KLF4 results in decreased lesion size, increased plaque stability, and a marked reduction in the number of VSMC-derived macrophage-like cells. Of particular interest in that study, in addition to an increase in macrophage and proinflammatory marker expression, KLF4 is induced in response to cholesterol loading in cultured VSMC. These observations led us to speculate that KLF4 is activated by metabolic stress triggered by perturbed intracellular lipid metabolism, such as cholesterol loading and altered LCFA composition, and if so, the AMPK/KLF4 axis plays a principal role in passing the metabolic stress on to the machinery regulating the phenotype of VSMC. Furthermore, the finding that an intracellular dysmetabolic state regulates KLF4 expression might best be viewed as evidence indicating that nutrient metabolism, cellular behavior, and cell cycle are intimately interconnected.[28]

A key question is how Elovl6 deficiency within VSMC results in a marked activation of AMPK. The classical view is that AMPK, a highly conserved heterotrimer comprising an α-catalytic subunit with $\beta\gamma$-regulatory subunits, responds to a reduction in the energy charge, switches off anabolic pathways such as fatty acid, triglyceride, and cholesterol synthesis, and switches on catabolic pathways that generate ATP, such as fatty acid oxidation and glycolysis.[24-26] However, activation of AMPK in Elovl6-deficient VSMC is not likely due to reduced cellular ATP content because exposure of cultured HASMC with palmitate recapitulated the response to Elovl6 knockdown. Thus, we propose that specific composition of LCFA, rather than reducing energy charge, induces the activation of AMPK in VSMC. In fact, Watt et al previously showed that palmitate treatment induces AMPK activation in L6 skeletal muscle myotubes in the absence of detectable changes in free AMP and glycogen content,[47] although precise molecular mechanisms whereby palmitate induces AMPK have not been described.

Our study newly identifies ROS as an upstream effector that induces AMPK activation in response to increased palmitate availability. We previously showed that dysregulation of Elovl6-mediated LCFA metabolism induces ROS production and pulmonary fibrosis.[13] Similar findings were observed in the present study, implying that ROS production in Elovl6-deficient cells is not cell type specific. We now demonstrate several lines of evidence indicating the causative role of ROS production for AMPK/KLF4 activation in Elovl6-deficient VSMC: (1) ROS production was increased in Elovl6$^{-/-}$ mice and siElovl6-transfected VSMC; (2) palmitate induced and oleate reduced ROS production; and (3) exposure of VSMC to H_2O_2 recapitulated the findings of Elovl6-deficient VSMC, including an increased phosphorylation of AMPK, elevation of KLF expression, and reduced VSMC gene expression. These data support the accumulating evidence indicating that increased ROS production in response to saturated LCFA overload plays a critical role in the regulation of cellular function.[48-51] Then, what are the mechanisms by which ROS induces AMPK activation? Although this question remains to be addressed, we recently found that the expression of Sestrin 1 and 2, which function as antioxidants or as AMPK activators in response to metabolic stress,[52] was increased in HASMC with Elovl6 knockdown. Future work should be warranted to identify the mechanism of ROS generation and ROS-induced AMPK activation in Elovl6-deficient VSMC.

Our results have potential clinical implications, especially related to the vascular complications in type 2 diabetes and obese subjects because previous studies showed that Elovl6 expression is transcriptionally induced by insulin and overnutrition through the action of the lipogenic transcription factor, SREBP1c[9,53] in hepatocytes. We found that PDGF-BB and hypoxia efficiently increased Elovl6 gene expression in

HASMC (Figures S3 and S10). Thus, it is tempting to speculate that overnutrition-induced elevation of Elovl6 expression in VSMC may contribute to the development of advanced atherosclerotic lesions and neointima by priming the cells for enhanced mitogenic response.

Our findings that mTOR and p21 expression was profoundly affected by Elovl6 knockdown seem to support the concept that growth and cell division are coordinately regulated to ensure that cells keep a fairly constant size.[54] Our study further highlights the central role of AMPK not only as a sensor for AMP/ATP levels but also as a sensor of metabolic stress caused by change in lipid composition. There has been a general consensus that AMPK activation directly and indirectly (via TSC2 and Raptor) suppresses mTOR activity to limit protein synthesis. Accordingly, our data corroborate the notion that AMPK is a regulator of cellular proliferation and protein synthesis by coordinating multiple cellular processes to maintain energy homeostasis and normal cellular function.

It is possible that activation of AMPK is expected to promote preferential partitioning of intracellular fatty acids away from esterification toward oxidation. Thus, activation of AMPK could be an endogenous protective mechanism to ameliorate lipotoxic effects of palmitate leading to endoplasmatic reticulum (ER) stress, inflammation, and insulin resistance[55–57] in Elovl6-deficient VSMC. Further studies are needed to verify our hypothesis that activation of AMPK/KLF4 signaling by loss of Elovl6 is protective against atherosclerosis by using double knockout mice of Elovl6 and apoE.

In summary, our study reveals a previously unrecognized role of Elovl6-driven LCFA metabolism as an intracellular cue for the regulation of VSMC phenotypic switching. Furthermore, we provide evidence for the role of LCFA composition and ROS production in the activation of AMPK/KLF4 signaling in VSMC. These findings indicate that strategies aimed at Elovl6-driven LCFA metabolism and AMPK/KLF4 signaling may represent a successful approach to limit atherosclerosis and postangioplasty restenosis.

Acknowledgments

The authors thank Miki Matsui, Takako Kobayashi, Keiko Arai, and Yukiyo Tosaka (Gunma University Graduate School of Medicine) for technical assistance. We also gratefully acknowledge Drs Masafumi Takahashi and Fumitake Usui (Jichi Medical University Center for Molecular Medicine) for technical support in the mouse femoral artery wire injury model.

Sources of Funding

This work was supported by a Grant-in-Aid for Scientific Research from the Japan Society for the Promotion of Science (to H.Sunaga, Matsui, Iso, Yokoyama, and Kurabayashi), Gunma University Initiative for Advanced Research (to Kurabayashi), and Japan Heart Foundation and Astellas Grant for Research on Atherosclerosis Update (to H.Sunaga, Matsui).

Disclosures

None.

References

1. Gomez D, Owens GK. Smooth muscle cell phenotypic switching in atherosclerosis. *Cardiovasc Res*. 2012;95:156–164.
2. Owens GK. Regulation of differentiation of vascular smooth muscle cells. *Physiol Rev*. 1995;75:487–517.
3. Bennett MR, Sinha S, Owens GK. Vascular smooth muscle cells in atherosclerosis. *Circ Res*. 2016;118:692–702.
4. Tabas I, Garcia-Cardena G, Owens GK. Recent insights into the cellular biology of atherosclerosis. *J Cell Biol*. 2015;209:13–22.
5. Gabbiani G, Schmid E, Winter S, Chaponnier C, de Ckhastonay C, Vandekerckhove J, Weber K, Franke WW. Vascular smooth muscle cells differ from other smooth muscle cells: predominance of vimentin filaments and a specific alpha-type actin. *Proc Natl Acad Sci USA*. 1981;78:298–302.
6. Allahverdian S, Chehroudi AC, McManus BM, Abraham T, Francis GA. Contribution of intimal smooth muscle cells to cholesterol accumulation and macrophage-like cells in human atherosclerosis. *Circulation*. 2014;129:1551–1559.
7. Feil S, Fehrenbacher B, Lukowski R, Essmann F, Schulze-Osthoff K, Schaller M, Feil R. Transdifferentiation of vascular smooth muscle cells to macrophage-like cells during atherogenesis. *Circ Res*. 2014;115:662–667.
8. Shankman LS, Gomez D, Cherepanova OA, Salmon M, Alencar GF, Haskins RM, Swiatlowska P, Newman AA, Greene ES, Straub AC, Isakson B, Randolph GJ, Owens GK. KLF4-dependent phenotypic modulation of smooth muscle cells has a key role in atherosclerotic plaque pathogenesis. *Nat Med*. 2015;21:628–637.
9. Moon YA, Shah NA, Mohapatra S, Warrington JA, Horton JD. Identification of a mammalian long chain fatty acyl elongase regulated by sterol regulatory element-binding proteins. *J Biol Chem*. 2001;276:45358–45366.
10. Matsuzaka T, Shimano H, Yahagi N, Kato T, Atsumi A, Yamamoto T, Inoue N, Ishikawa M, Okada S, Ishigaki N, Iwasaki H, Iwasaki Y, Karasawa T, Kumadaki S, Matsui T, Sekiya M, Ohashi K, Hasty AH, Nakagawa Y, Takahashi A, Suzuki H, Yatoh S, Sone H, Toyoshima H, Osuga J, Yamada N. Crucial role of a long-chain fatty acid elongase, Elovl6, in obesity-induced insulin resistance. *Nat Med*. 2007;13:1193–1202.
11. Matsuzaka T, Atsumi A, Matsumori R, Nie T, Shinozaki H, Suzuki-Kemuriyama N, Kuba M, Nakagawa Y, Ishii K, Shimada M, Kobayashi K, Yatoh S, Takahashi A, Takekoshi K, Sone H, Yahagi N, Suzuki H, Murata S, Nakamuta M, Yamada N, Shimano H. Elovl6 promotes nonalcoholic steatohepatitis. *Hepatology*. 2012;56:2199–2208.
12. Saito R, Matsuzaka T, Karasawa T, Sekiya M, Okada N, Igarashi M, Matsumori R, Ishii K, Nakagawa Y, Iwasaki H, Kobayashi K, Yatoh S, Takahashi A, Sone H, Suzuki H, Yahagi N, Yamada N, Shimano H. Macrophage Elovl6 deficiency ameliorates foam cell formation and reduces atherosclerosis in low-density lipoprotein receptor-deficient mice. *Arterioscler Thromb Vasc Biol*. 2011;31:1973–1979.
13. Sunaga H, Matsui H, Ueno M, Maeno T, Iso T, Syamsunarno MR, Anjo S, Matsuzaka T, Shimano H, Yokoyama T, Kurabayashi M. Deranged fatty acid composition causes pulmonary fibrosis in Elovl6-deficient mice. *Nat Commun*. 2013;4:2563.
14. Sata M, Maejima Y, Adachi F, Fukino K, Saiura A, Sugiura S, Aoyagi T, Imai Y, Kurihara H, Kimura K, Omata M, Makuuchi M, Hirata Y, Nagai R. A mouse model of vascular injury that induces rapid onset of medial cell apoptosis followed by reproducible neointimal hyperplasia. *J Mol Cell Cardiol*. 2000;32:2097–2104.
15. Daniel JM, Bielenberg W, Stieger P, Weinert S, Tillmanns H, Sedding DG. Time-course analysis on the differentiation of bone marrow-derived progenitor cells into smooth muscle cells during neointima formation. *Arterioscler Thromb Vasc Biol*. 2010;30:1890–1896.
16. Doi H, Iso T, Yamazaki M, Akiyama H, Kanai H, Sato H, Kawai-Kowase K, Tanaka T, Maeno T, Okamoto E, Arai M, Kedes L, Kurabayashi M. HERP1 inhibits myocardin-induced vascular smooth muscle cell differentiation by

interfering with SRF binding to CArG box. *Arterioscler Thromb Vasc Biol*. 2005;25:2328–2334.

17. He TC, Zhou S, da Costa LT, Yu J, Kinzler KW, Vogelstein B. A simplified system for generating recombinant adenoviruses. *Proc Natl Acad Sci USA*. 1998;95:2509–2514.
18. Farhat MY, Vargas R, Dingaan B, Ramwell PW. In vitro effect of oestradiol on thymidine uptake in pulmonary vascular smooth muscle cell: role of the endothelium. *Br J Pharmacol*. 1992;107:679–683.
19. Aoyagi-Ikeda K, Maeno T, Matsui H, Ueno M, Hara K, Aoki Y, Aoki F, Shimizu T, Doi H, Kawai-Kowase K, Iso T, Suga T, Arai M, Kurabayashi M. Notch induces myofibroblast differentiation of alveolar epithelial cells via transforming growth factor-β-Smad3 pathway. *Am J Respir Cell Mol Biol*. 2011;45:136–144.
20. Bligh EG, Dyer WJ. A rapid method of total lipid extraction and purification. *Can J Biochem Physiol*. 1959;37:911–917.
21. Scholzen T, Gerdes J. The Ki-67 protein: from the known and the unknown. *J Cell Physiol*. 2000;182:311–322.
22. Hardie DG. AMPK and Raptor: matching cell growth to energy supply. *Mol Cell*. 2008;30:263–265.
23. el-Deiry WS, Tokino T, Velculescu VE, Levy DB, Parsons R, Trent JM, Lin D, Mercer WE, Kinzler KW, Vogelstein B. WAF1, a potential mediator of p53 tumor suppression. *Cell*. 1993;75:817–825.
24. Carling D. The AMP-activated protein kinase cascade—a unifying system for energy control. *Trends Biochem Sci*. 2004;29:18–24.
25. Hardie DG. AMP-activated/SNF1 protein kinases: conserved guardians of cellular energy. *Nat Rev Mol Cell Biol*. 2007;8:774–785.
26. Kahn BB, Alquier T, Carling D, Hardie DG. AMP-activated protein kinase: ancient energy gauge provides clues to modern understanding of metabolism. *Cell Metab*. 2005;1:15–25.
27. Igata M, Motoshima H, Tsuruzoe K, Kojima K, Matsumura T, Kondo T, Taguchi T, Nakamaru K, Yano M, Kukidome D, Matsumoto K, Toyonaga T, Asano T, Nishikawa T, Araki E. Adenosine monophosphate-activated protein kinase suppresses vascular smooth muscle cell proliferation through the inhibition of cell cycle progression. *Circ Res*. 2005;97:837–844.
28. Jones RG, Plas DR, Kubek S, Buzzai M, Mu J, Xu Y, Birnbaum MJ, Thompson CB. AMP-activated protein kinase induces a p53-dependent metabolic checkpoint. *Mol Cell*. 2005;18:283–293.
29. Hardie DG. The AMP-activated protein kinase pathway—new players upstream and downstream. *J Cell Sci*. 2004;117:5479–5487.
30. Kerner J, Hoppel C. Fatty acid import into mitochondria. *Biochim Biophys Acta*. 2000;1486:1–17.
31. Desvergne B, Wahli W. Peroxisome proliferator-activated receptors: nuclear control of metabolism. *Endocr Rev*. 1999;20:649–688.
32. Hardy S, Langelier Y, Prentki M. Oleate activates phosphatidylinositol 3-kinase and promotes proliferation and reduces apoptosis of MDA-MB-231 breast cancer cells, whereas palmitate has opposite effects. *Cancer Res*. 2000;60:6353–6358.
33. Li S, Zhou T, Li C, Dai Z, Che D, Yao Y, Li L, Ma J, Yang X, Gao G. High metastatic gastric and breast cancer cells consume oleic acid in an AMPK dependent manner. *PLoS One*. 2014;9:e97330.
34. Lu G, Meier KE, Jaffa AA, Rosenzweig SA, Egan BM. Oleic acid and angiotensin II induce a synergistic mitogenic response in vascular smooth muscle cells. *Hypertension*. 1998;31:978–985.
35. Evert M, Calvisi DF, Evert K, De Murtas V, Gasparetti G, Mattu S, Destefanis G, Ladu S, Zimmermann A, Delogu S, Thiel S, Thiele A, Ribback S, Dombrowski F. V-AKT murine thymoma viral oncogene homolog/mammalian target of rapamycin activation induces a module of metabolic changes contributing to growth in insulin-induced hepatocarcinogenesis. *Hepatology*. 2012;55:1473–1484.
36. Takahashi K, Yamanaka S. Induction of pluripotent stem cells from mouse embryonic and adult fibroblast cultures by defined factors. *Cell*. 2006;126:663–676.
37. Adam PJ, Regan CP, Hautmann MB, Owens GK. Positive- and negative-acting Krüppel-like transcription factors bind a transforming growth factor β control element required for expression of the smooth muscle cell differentiation marker SM22α in vivo. *J Biol Chem*. 2000;275:37798–37806.
38. Yoshida T, Kaestner KH, Owens GK. Conditional deletion of Krüppel-like factor 4 delays downregulation of smooth muscle cell differentiation markers but accelerates neointimal formation following vascular injury. *Circ Res*. 2008;102:1548–1557.
39. Liu Y, Sinha S, McDonald OG, Shang Y, Hoofnagle MH, Owens GK. Kruppel-like factor 4 abrogates myocardin-induced activation of smooth muscle gene expression. *J Biol Chem*. 2005;280:9719–9727.
40. Pidkovka NA, Cherepanova OA, Yoshida T, Alexander MR, Deaton RA, Thomas JA, Leitinger N, Owens GK. Oxidized phospholipids induce phenotypic switching of vascular smooth muscle cells in vivo and in vitro. *Circ Res*. 2007;101:792–801.
41. Dang DT, Chen X, Feng J, Torbenson M, Dang LH, Yang VW. Overexpression of Krüppel-like factor 4 in the human colon cancer cell line RKO leads to reduced tumorigenecity. *Oncogene*. 2003;22:3424–3430.
42. Shields JM, Christy RJ, Yang VW. Identification and characterization of a gene encoding a gut-enriched Kruppel-like factor expressed during growth arrest. *J Biol Chem*. 1996;271:20009–20017.
43. Zhang W, Geiman DE, Shields JM, Dang DT, Mahatan CS, Kaestner KH, Biggs JR, Kraft AS, Yang VW. The gut-enriched Krüppel-like factor (Krüppel-like factor 4) mediates the transactivating effect of p53 on the $p21^{WAF1/Cip1}$ promoter. *J Biol Chem*. 2000;275:18391–18398.
44. Wang Y, Zhao B, Zhang Y, Tang Z, Shen Q, Zhang W, Du J, Chien S, Wang N. Krüppel-like factor 4 is induced by rapamycin and mediates the anti-proliferative effect of rapamycin in rat carotid arteries after balloon injury. *Br J Pharmacol*. 2012;165:2378–2388.
45. Collado M, Blasco MA, Serrano M. Cellular senescence in cancer and aging. *Cell*. 2007;130:223–233.
46. Wiley CD, Campisi J. From ancient pathways to aging cells—connecting metabolism and cellular senescence. *Cell Metab*. 2016;23:1013–1021.
47. Watt MJ, Steinberg GR, Chen ZP, Kemp BE, Febbraio MA. Fatty acids stimulate AMP-activated protein kinase and enhance fatty acid oxidation in L6 myotubes. *J Physiol*. 2006;574:139–147.
48. Shen H, Eguchi K, Kono N, Fujiu K, Matsumoto S, Shibata M, Oishi-Tanaka Y, Komuro I, Arai H, Nagai R, Manabe I. Saturated fatty acid palmitate aggravates neointima formation by promoting smooth muscle phenotypic modulation. *Arterioscler Thromb Vasc Biol*. 2013;33:2596–2607.
49. Wang X, Liu JZ, Hu JX, Wu H, Li YL, Chen HL, Bai H, Hai CX. ROS-activated p38 MAPK/ERK-AKT cascade plays a central role in palmitic acid-stimulated hepatocyte proliferation. *Free Radic Biol Med*. 2011;51:539–551.
50. Lee CH, Lee SD, Ou HC, Lai SC, Cheng YJ. Eicosapentaenoic acid protects against palmitic acid-induced endothelial dysfunction via activation of the AMPK/eNOS pathway. *Int J Mol Sci*. 2014;15:10334–10349.
51. Kim JE, Kim YW, Lee IK, Kim JY, Kang YJ, Park SY. AMP-activated protein kinase activation by 5-aminoimidazole-4-carboxamide-1-beta-D-ribofuranoside (AICAR) inhibits palmitate-induced endothelial cell apoptosis through reactive oxygen species suppression. *J Pharmacol Sci*. 2008;106:394–403.
52. Lee JH, Budanov AV, Karin M. Sestrins orchestrate cellular metabolism to attenuate aging. *Cell Metab*. 2013;18:792–801.
53. Matsuzaka T, Shimano H, Yahagi N, Yoshikawa T, Amemiya-Kudo M, Hasty AH, Okazaki H, Tamura Y, Iizuka Y, Ohashi K, Osuga J, Takahashi A, Yato S, Sone H, Ishibashi S, Yamada N. Cloning and characterization of a mammalian fatty acyl-CoA elongase as a lipogenic enzyme regulated by SREBPs. *J Lipid Res*. 2002;43:911–920.
54. Neufeld TP, Edgar BA. Connections between growth and the cell cycle. *Curr Opin Cell Biol*. 1998;10:784–790.
55. Staiger H, Staiger K, Stefan N, Wahl HG, Machicao F, Kellerer M, Haring HU. Palmitate-induced interleukin-6 expression in human coronary artery endothelial cells. *Diabetes*. 2004;53:3209–3216.
56. Staiger K, Staiger H, Weigert C, Haas C, Haring HU, Kellerer M. Saturated, but not unsaturated, fatty acids induce apoptosis of human coronary artery endothelial cells via nuclear factor-κB activation. *Diabetes*. 2006;55:3121–3126.
57. Weigert C, Brodbeck K, Staiger H, Kausch C, Machicao F, Haring HU, Schleicher ED. Palmitate, but not unsaturated fatty acids, induces the expression of interleukin-6 in human myotubes through proteasome-dependent activation of nuclear factor-κB. *J Biol Chem*. 2004;279:23942–23952.

SUPPLEMENTAL MATERIAL

Data S1. Supplemental Experimental Procedures

Animals

C57BL/6 strain (wild-type, WT) mice and Wistar rats were purchased from CLEA Japan Inc.. *Elovl6*$^{-/-}$ mice were kindly gifted from Dr. H. Shimano (Tsukuba University). These mice were intercrossed into *Elovl6*$^{-/-}$ or *Elovl6*$^{-/+}$ mice. Littermates were genotyped by PCR.

Human arterial tissue

Eight human coronary artery sections, containing diffuse intimal thickening or apparently normal pathology, were obtained from patients with ischemic or non-ischemic heart disease.

Tissue preparation and immunohistochemistry

Following the induction of deep anesthesia, mice were killed and perfused via the left ventricle with phosphate buffered saline (PBS), followed by perfusion fixation with 10% formalin for 10 min. The right femoral artery was carefully harvested and embedded in paraffin. Human arterial tissues were obtained from patients at autopsy and tissue samples were fixed in formalin and embedded in paraffin. Each serial section (4-μm) was prepared for the histological analysis.

Sections were deparaffinized in xylene and rehydrated prior to antigen retrieval by boiling in citrate buffer. Elovl6 (ABGENT, AP6524a, 1:50), SMα-actin (Dako corp., M0851, 1:500), and Nitrotyrosine (Cell Signaling Technology, #9691, 1:50) staining was performed using the Vectastain Elite ABC kit (Vector Laboratories) according to the manufacturer's instruction, with 3,3'-diaminobenzidine (DAB) as the chromogenic substrate. Sections were stained with hematoxylin and eosin (H&E) and elastica van Gieson (EVG) using standard procedures. The immunohistochemistry of artery cross-sections was examined by an image analysis

(WinROOF, Mitani Shoji Co.). In each artery, measurements of the intimal (I, tissue between the lumen and internal elastic lamina) and medial (M, tissue between the internal and external elastic lamina) areas were obtained, and the intimal/media area ratio (I/M ratio) was calculated[1-3]. Ki-67 (Thermo Scientific, SP6, 1:200) -positive cells were calculated as the number of cells that co-localized with 4', 6-diamidino-2-phenylindole (DAPI, Dojindo, 1:1000) in the neointimal thickening area of the femoral artery in mice.

Balloon injury to the rat carotid artery

The carotid artery of rats was injured with a balloon as described previously[4]. In brief, 8-week-old male Wister (n=12) rats weighing approximately 300 g were injured with a 2F balloon catheter (Edwards Lifesciences). The animals were euthanized 14 days after the balloon injury and the thoracic aorta was harvested.

Cell culture

Human aortic smooth muscle cells (HASMC) were purchased from Kurabo Ltd. HASMC were cultured at 37°C in a 5% CO_2 atmosphere in Humedia-SB2 medium supplemented with 5% fetal bovine serum (FBS), 0.5 μg/ml of recombinant human epidermal growth factor (EGF), 2 μg/ml of recombinant human basic fibroblast growth factor (bFGF), 5 mg/ml of insulin, 50 mg/ml of gentamycin, and 50 μg/ml of amphotericin B. HASMC were used between passages 4 and 8 in these experiments. Serum-starved HASMC with 0.1% BSA (24 hours) were incubated in the presence or absence of BSA-conjugated palmitate or oleate (Sigma, 250 μM). Serum-starved HASMC were also treated with 1 mM AICAR (Toronto Research Chemicals) or 10 μM Compound C (Merck). Cells were also treated with vehicle as control, TGF-β （Roche）or PDGF-BB (R&D systems). HASMC was treated with 100 μM H_2O_2 (Wako) in the presence or absence of 1 unit catalase (Merck Millipore).

RNA isolation and quantitative real-time reverse transcription (qRT-PCR)

Total RNA was extracted from the mouse aorta and cultured HASMC using ISOGEN regent (Takara Bio) according to the manufacturer's protocol. One microgram of RNA was used for reverse transcription with the RNA LA PCR Kit (Takara Bio) and qRT-PCR analysis was performed using the THUNDERBIRD SYBR qPCR Mix (TOYOBO) according to the manufacturers' protocols. QPCR was carried out using a MX3000P quantitative system (Stratagene). All primer sequences are shown in Supplemental Table I and Table II. Each experiment used three samples and was performed three times.

Construction of siRNA oligonucleotides and transfection

siRNA oligonucleotides (human siElovl6: CUU UUG AAC AGA AGA GUA AAU, human sip21: CGA CUG UGA UGC GCU AAU G, CCU AAU CCG CCC ACA GGA A, CGU CAG AAC CCA UGC GGC A, AGA CCA GCA UGA CAG AUU U, human siKLF4: CCA GAG GAG CCC AAG CCA ATT, siGFP: GUU CAG CGU GUC CGG CGA GTT) were purchased from BONAC Corporation and transfected with Lipofectamine RNAiMAX Regent (Invitrogen) according to the manufacturer's protocol. siGFP concentration used was 50 nM, which has little, if any, off-target effects[5]. In order to effectively inhibit the four transcript variants of human p21 expression, we used four sequences of p21 siRNA that were mixed in equal amounts.

[^{3}H]-thymidine uptake

The uptake of radiolabeled [^{3}H]-thymidine was assayed as described previously[6], with some modifications. Briefly, HASMC were seeded on 24-well plates (2.5×10^4 cells/well) and cultured for 24 hours in Hu-media containing 5% FBS. These cells were treated with each adenovirus or siRNA followed by serum-starvation (0.5% FBS) for 24 hours. Serum-starved HASMC with 0.1% BSA (24 hours) were also treated with BSA-

conjugated palmitate or oleate (250 μM each) for 24 hours. The cells were incubated with [^{3}H]-thymidine (1 mCi/well; Perkin Elmer) in a 5% CO_2 atmosphere at 37°C. After a 5 hours incubation, the cells were washed with ice-cold PBS and the reaction was stopped by the addition of ice-cold 5% trichloroacetic acid (TCA) for 30 min. The cells were digested in 0.5 M NaOH for 1 hour and aliquots were used to determine the radioactive count with a scintillator counter (Aloca LSC3000).

Scratch wound healing assay

The measurement of migration by the scratch mobility assay was performed as described previously[7]. Briefly, HASMC transduced with the adenovirus or siRNA were seeded on 6-well plates. After 24 hours, a single uniform scratch was made on the monolayer in each well using a sterile 200-μl pipette tip. The monolayer was rinsed three times and placed in Hu-media with 0.5% FBS. Phase contrast images were captured immediately and after 8 hours or 24 hours incubation, and a digital image of the scar was taken at a magnification of ×40. Each experiment was performed in duplicate and three independent assays were performed (n=6).

Boyden chamber assay

Boyden chamber assay was performed as previously described[7]. Briefly, HASMC which were transfected with siElovl6 or siGFP for 48 h were plated (2.5×10^4/well) in the upper chamber of transwells (6.5-mm diameter, 5.0-μm pore size polycarbonate membrane, Neuro Probe). The cells were returned to the 37°C 5% CO_2 incubator for 4 h, rinsed with PBS, and cells remaining at the top of the polycarbonate membrane were removed. The cells that had migrated through pores to the lower surface were fixed in methanol, stained with a Diff-Quick kit (Sysmex). Membranes were mounted on microslides and four random microscopic fields per well were quantified. Each experiment was conducted in duplicate and three separate experiments were performed (n=6-

7).

Fatty acid composition

Lipids from the mouse aorta and HASMC were extracted using the Bligh and Dyer method as described previously[8]. Briefly, arterial tissues and cells were extracted with chloroform/methanol (1:2, v/v) solution. In order to break monophase, 1 M NaCl solution and chloroform were then added, and incubated on ice for 10 min. After centrifugation at 2,000 rpm for 5 min, the aqueous solution was discarded and the chloroform phase was transferred to a test tube. The chloroform phase was evaporated using nitrogen gas, and the lipids obtained were subjected to a fatty acid composition analysis at an external laboratory (SRL Inc.).

Western blot analysis

Tissue samples and cells were homogenized on ice in RIPA buffer (20 mM Tris-HCl [pH 7.4], 150 mM NaCl, 1% NP-40, 1% sodium deoxycholate, 0.1% SDS, and containing complete mini and phosSTOP solution (Roche)). The mixture was centrifuged at 15,000 rpm for 30 min and the supernatant was subjected to SDS-PAGE. Protein concentrations were determined by the Bradford method using a colorimetric assay (Bio-Rad). Western blot analysis was performed according to standard procedures using the following primary antibodies: rabbit monoclonal phospho-AMPK (Cell Signaling Technology, #2535, 1:250), AMPK (Cell Signaling Technology, #2603, 1:500), ACC (Cell Signaling Technology, #3676, 1:500), phospho-mTOR (Cell Signaling Technology, #5536, 1:250), mTOR (Cell Signaling Technology, #2983, 1:500), p21 (Cell Signaling Technology, #2947, 1:500), KLF4 (Cell Signaling Technology, #4038, 1:250), β-actin (Cell Signaling Technology, #4970, 1:500), and rabbit polyclonal phospho-ACC (Cell Signaling Technology, #3661, 1:250), phospho-p53 (Cell Signaling Technology, #9284, 1:250), SMα-actin (Dako corp., M0851, 1:100), SM22α (Abcam, ab14106,

1:1000) and mouse polyclonal p53 (Santa Cruz Biotechnology, #Sc-126, 1:100). Antigens were revealed by Immobilon Western HRP Substrate (Millipore) after an incubation with horseradish peroxidase-conjugated anti-rabbit or mouse IgG. The density of a band was quantified using ImageJ software.

Preparation of fatty acid solution

Palmitate was conjugated to fatty acid-free bovine serum albumin at a 3.5:1 molar ratio by dissolving them in ethanol and mixing with an aqueous BSA solution (BSA in phosphate-buffered saline, PBS) at 37°C until homogeneous. They were then passed through a 0.2-μM filter.

Estimation of ROS generation

Intracellular ROS levels were detected with the oxidant-sensitive fluorogenic probes 5-(and 6)-chloromethyl-2',7'-dichlorodihydrofluorescein diacetate, acetyl ester (CM-H_2DCFDA, Invitrogen). siRNA-transfected HASMC was incubated with 10 μM CM-H_2DCFDA in serum-free medium for 30 min at 37°C. Otherwise, the cells were incubated in the presence or absence of palmitic acid and oleic acid for 15 min after 30 min incubation of 10 μM CM-H_2DCFDA. After incubation at 37°C, fluorescence was detected.

Ethical approval

Human coronary artery tissues with atherosclerosis were obtained from patients at autopsy with written informed consent of their family at Gunma University Hospital. This protocol was approved by the Institutional Review Board at the Gunma University Hospital.

Figure S1. Expression of Elovl6 in intimal thickening lesions of the human coronary artery.

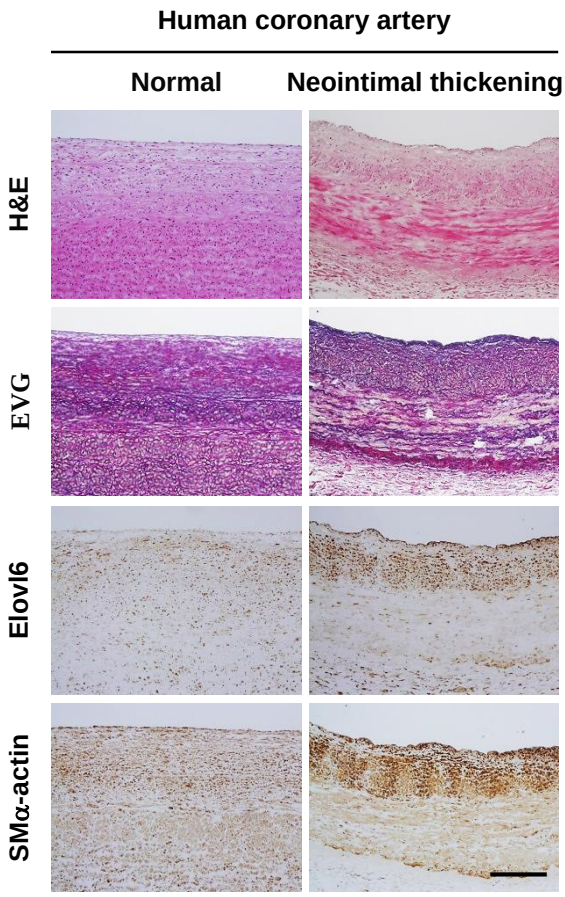

Eight human coronary artery sections, containing diffuse intimal thickening or apparently normal pathology, from a patient with ischemic or non-ischemic heart disease were stained with H&E, EVG, and with antibodies against Elovl6 and SMα-actin. The expression of Elovl6 was co-localized with SMα-actin in the thin medial layer in a normal coronary artery, and increased in intimal thickening lesions of human coronary artery. Scale bar = 200 μm. H&E, hematoxylin-eosin; EVG, elastica van Gieson; Elovl6, elongation of long-chain fatty acid family member 6; SMα-actin, smooth muscle alpha-actin.

Figure S2. Adenovirus-mediated overexpression of Elovl6 in HASMC.

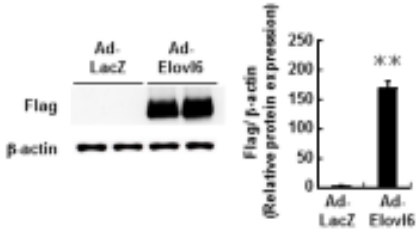

Western blot analysis with an anti-flag M2 antibody in HASMC transduced with Ad-Elovl6 (n=6) or Ad-LacZ (n=6). Flag-tagged Elovl6 was markedly up-regulated in HASMC infected with Ad-Elovl6. β-actin was measured as an internal control. This experiment was performed at least three times. Values are represented as the means ± SEM of three experiments. *$p<0.05$, **$p<0.01$, as measured by the Mann-Whitney U-test. HASMC, human aortic smooth muscle cells; Ad-LacZ, adenoviral vector encoding lacZ gene; Ad-Elovl6, adenoviral vector encoding elongation of long-chain fatty acid family member 6 gene.

Figure S3. Induction of Elovl6 expression by PDGF-BB in HASMC.

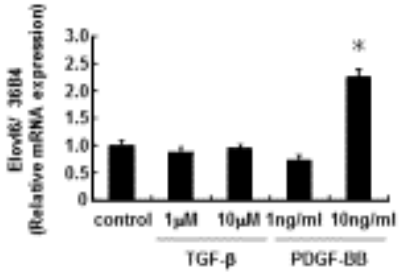

qRT-PCR for Elovl6 mRNA in HASMC. PDGF-BB induced Elovl6 mRNA levels in a dose-dependent manner (control, TGF-β, PDGF-BB: n=6). 36B4 mRNA levels were measured as internal controls. This experiment was performed at least three times. Values are represented as the means ± SEM of three experiments. *$p<0.05$, as measured by the Tukey-Kramer test. Elovl6, elongation of long-chain fatty acid family member 6; HASMC, human aortic smooth muscle cells; PDGF-BB, platelet-derived growth factor-BB, TGF-β, transforming growth factor-beta.

Figure S4. Overexpression of Elovl6 modulated cell cycle regulators in HASMC.

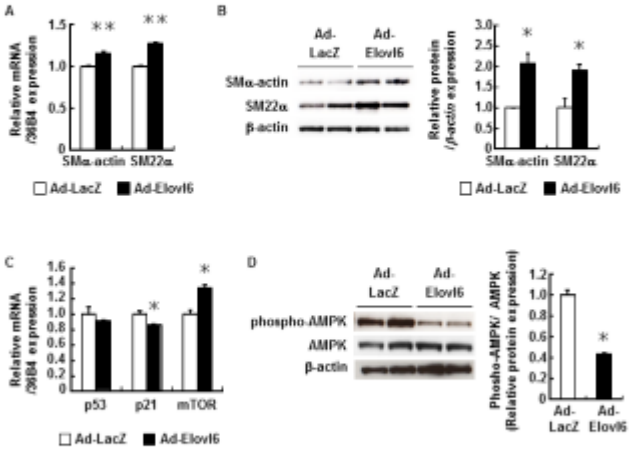

(A, B) qRT-PCR for SMα-actin and SM22α mRNA levels (A) and western blot assay for protein levels (B) in HASMC infected with Ad-Elovl6 (n=6) or Ad-LacZ (n=5) for 48 hours. Overexpression of Elovl6 increased the SM22α and SMα-actin mRNA and protein levels in HASMC. (C) qRT-PCR for the expression of p53, p21 and mTOR mRNA in HASMC infected with Ad-Elovl6 (n=6) or Ad-LacZ (n=7) for 48 hours. p21 mRNA levels were decreased while mTOR mRNA levels were increased by Elovl6 overexpression. (D) Western blot analysis of AMPK in HASMC infected with Ad-Elovl6 (n=6) or Ad-LacZ (n=6) for 48 hours. Overexpression of Elovl6 suppressed phosphorylation of AMPK. 36B4 for qRT-PCR and β-actin for western blot were measured as an internal control. Western blot data for the phosphorylation of AMPK were normalized by total AMPK in the

same samples, and expressed as a fold increase from the mean level of control group. Each experiment was performed at least three times. All values are represented as the means ± SEM of three experiments. *$p<0.05$, **$p<0.01$, as measured by the Mann-Whitney U-test. SMα-actin, smooth muscle alpha-actin; SM22α, smooth muscle protein 22-alpha; HASMC, human aortic smooth muscle cells; Ad-LacZ, adenoviral vector encoding lacZ gene; Ad-Elovl6, adenoviral vector encoding elongation of long-chain fatty acid family member 6 gene; mTOR, mammalian target of rapamycin; AMPK, AMP-activated protein kinase.

Figure S5. Elovl6-overexpression altered the fatty acid composition in HASMC.

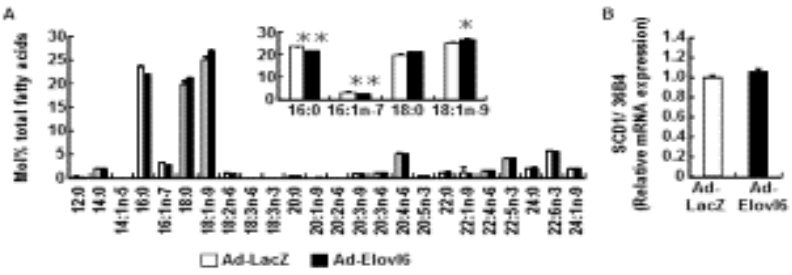

(A) Fatty acid composition of the neutral lipid extract from HASMC infected with Ad-Elovl6 (n=5) or Ad-LacZ (n=4) for 48 hours. The adenovirus-mediated overexpression of Elovl6 decreased the relative amounts of palmitate (C16:0) and palmitoleate (C16:1 n-7), and increased those of oleate (C18:1 n-9) more than the infection with Ad-LacZ. (B) qRT-PCR for SCD1 mRNA in HASMC infected with Ad-Elovl6 (n=6) or Ad-LacZ (n=5). The overexpression of Elovl6 did not change SCD1 mRNA levels. 36B4 was measured as an internal control. mRNA levels in the Ad-LacZ control group were normalized to a value of 1, while those in Ad-Elovl6 cells are shown relative to the control level. Each experiment was performed at least three times. All values are

represented as the means ± SEM of three experiments. *p<0.05, **p<0.01, as measured by the Mann-Whitney U-test. HASMC, human aortic smooth muscle cells; Ad-LacZ, adenoviral vector encoding lacZ gene; Ad-Elovl6, adenoviral vector encoding elongation of long-chain fatty acid family member 6 gene; SCD1, stearoyl-CoA desaturase 1.

Figure S6. Changes of Elovl6 expression in HASMC affect KLF4 expression.

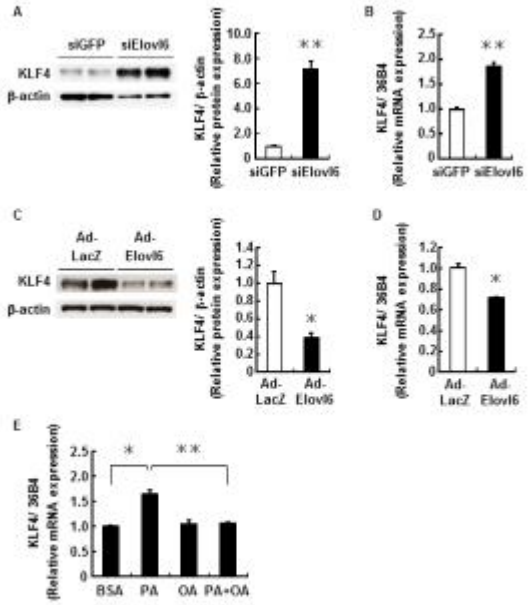

(A) Western blot analysis of KLF4 expression in HASMC transfected with Elovl6 (n=6) or GFP siRNA (n=6). KLF4 protein levels were significantly increased by the siRNA-mediated knockdown of Elovl6. (B) qRT-PCR analysis for KLF4 mRNA in HASMC with siRNA-mediated knockdown of Elovl6 (siGFP: n=7 ; siElovl6 : n=6). (C) Western blot analysis of KLF4 in HASMC infected with Ad-Elovl6 (n=6) or Ad-LacZ (n=6) for 48 hours. Overexpression of Elovl6 significantly decreased KLF4 protein levels. (D) qRT-PCR for KLF4 mRNA in HASMC infected with Ad-Elovl6 (n=6) or Ad-LacZ (n=6) for 48 hours. KLF4 mRNA levels were decreased by Elovl6 overexpression. (E) qRT-PCR for KLF4 mRNA in HASMC treated with fatty acids. The PA (C16:0) treatment significantly increased the KLF4 mRNA levels, whereas the OA (C18:1n-9) treatment inhibited this induction (BSA: n=8; PA, OA, PA + OA: n=7). 36B4 for qRT-PCR and β-actin for western blot were measured

as an internal control. Each experiment was performed at least three times. All values are represented as the means ± SEM of three experiments. *$p<0.05$, **$p<0.01$, as measured by the Mann-Whitney U-test (A-D) or Tukey-Kramer test (E). KLF4, krüppel-like factor 4; HASMC, human aortic smooth muscle cells; Ad-LacZ, adenoviral vector encoding lacZ gene; Ad-Elovl6, adenoviral vector encoding elongation of long-chain fatty acid family member 6 gene; PA, palmitic acid; OA, oleic acid; BSA, fatty acid-free bovine serum albumin.

Figure S7. Depletion of KLF4 affects cell cycle regulators and proliferation in HASMC with or without Elovl6 knockdown.

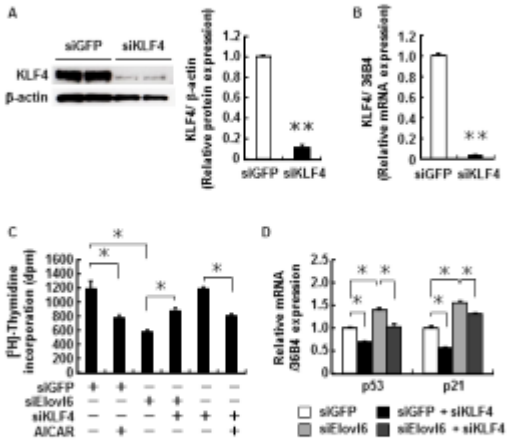

(A, B) Western blot analysis (A) or qRT-PCR (B) of KLF4 expression in HASMC transfected with KLF4 (n=6) or GFP siRNA (n=5). KLF4 expression was significantly decreased by the siRNA-mediated knockdown of KLF4. (C) [^{3}H]-thymidine uptake assay in HASMC transfected with Elovl6, KLF4 or GFP siRNA in the presence or absence of 1mM AICAR. Concomitant treatment of siKLF4 and siElovl6 partially reversed siElovl6-triggered inhibition of VSMC proliferation (siGFP, siElovl6, siKLF4: n=6; siElovl6 + siKLF4: n=7; AICAR: n=5). (D) Effects of KLF4 gene silencing on Elovl6 siRNA-induced cell cycle regulatory proteins in HASMC by qRT-PCR. Elovl6 depletion-induced expression of p53 and p21 was cancelled by the siRNA-

mediated knockdown of KLF4 (siGFP, siElovl6: n=6; siGFP or siElovl6 + siKLF4: n=7). Each experiment was performed at least three times. All values are represented as the means ± SEM of three experiments. *$p<0.05$, **$p<0.01$, as measured by the Mann-Whitney U-test (A, B) or Tukey-Kramer test (C, D). KLF4, krüppel-like factor 4; HASMC, human aortic smooth muscle cells; AICAR, 5-aminoimidazole-4-carboxamide ribonucleotide; Elovl6, elongation of long-chain fatty acid family member 6; VSMC, vascular smooth muscle cells.

Figure S8. KLF4 knockdown affects SMC marker gene expression in a context-depend manner.

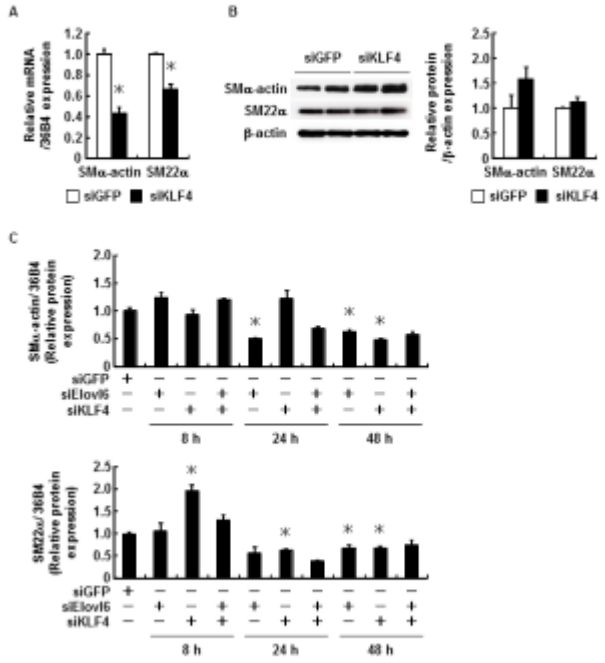

(A, B) qRT-PCR for SMα-actin and SM22α mRNA (A) and western blot assay for protein (B) in HASMC transfected with KLF4. SMα-actin and SM22α mRNA levels were significantly decreased, but protein levels were not changed by siRNA-mediated knockdown of KLF4 (siGFP: n=7; siKLF4: n=8). 36B4 for qRT-PCR and β-actin for western blot were measured as an internal control. (C) qRT-PCR for the time-course of SMα-actin or SM22α mRNA levels, normalized by mRNA levels of 36B4, in HASMC transfected with siRNA targeting Elovl6 or KLF4. siRNA-mediated Elovl6 or KLF4 knockdown increased SMα-actin or SM22α expressions at an early time (8-24h), however, Elovl6 or KLF4 knockdown markedly suppressed SMC marker gene expressions 48 h after transfection (siGFP, siElovl6, siKLF4 : n=7 ; siElovl6 + siKLF4 : n=7). Each

experiment was performed at least three times. All values are represented as the means ± SEM of three experiments. *p<0.05, **p<0.01, as measured by the Mann-Whitney U-test (A, B) or Tukey-Kramer test (C). SMα-actin, smooth muscle alpha-actin; SM22α, smooth muscle protein 22-alpha; HASMC, human aortic smooth muscle cells; KLF4, krüppel-like factor 4; Elovl6, elongation of long-chain fatty acid family member 6; SMC, smooth muscle cell.

Figure S9. KLF4 knockdown had no effects on phosphorylation of AMPK.

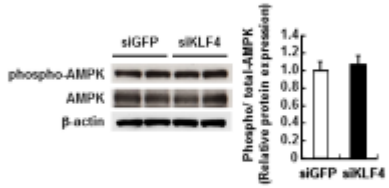

Western blot analysis of AMPK phosphorylation in HASMC transfected with KLF4 (n=6) or GFP siRNA (n=5). Phosphorylation of AMPK was not changed by siRNA-mediated knockdown of KLF4. β-actin was measured as an internal control. This experiment was performed at least three times. All values are represented as the means ± SEM of three experiments, measured by the Mann-Whitney U-test. AMPK, AMP-activated protein kinase; HASMC, human aortic smooth muscle cells; KLF4, krüppel-like factor 4.

Figure S10. Induction of Elovl6 expression by hypoxic stress in HASMC.

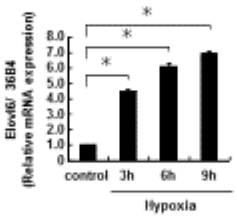

qRT-PCR for Elovl6 mRNA in HASMC. Hypoxic stress markedly induced Elovl6 mRNA levels, normalized by mRNA levels of 36B4, in a time-dependent manner (control, hypoxia: n=6). This experiment was performed at least three times. Values are represented as the means ± SEM of three experiments. *$p<0.05$, as measured by the Tukey-Kramer test. Elovl6, elongation of long-chain fatty acid family member 6; HASMC, human aortic smooth muscle cells.

Table S1. Human primer sequences used for qRT-PCR

Target (Human)	Sense	Anti-sense
Elovl6	5’-CGAGAATGAAGCCATCCAAT-3’	5’-CCCGCAAGGCATAGTAAGAG-3
SCD1	5’-CCACCGCTCTTACAAAGCTC-3’	5’-TAGTTGTGGAAGCCCTCACC-3
SMα-actin	5’-ATGAGGGCTATGCCTTGCCC-3’	5’-CCCGATGAAGGATGGCTGGA-3’
SM22α	5’-AACAGCCTGTACCCTGATGG-3’	5’-ATGACATGCTTTCCCTCCTG-3’
p53	5’-GTGGAAGGAAATTTGCGTGT-3’	5’-TCTGAGTCAGGCCCTTCTGT-3
p21	5’-GAGCGATGGAACTTCGACTT-3	5’-GGCGTTTGGAGTGGTAGAAA-3
mTOR	5’-AGTGGACCAGTGGAAACAGG-3	5’-TCCGGCTGCTGCTGTAGCTTATT-3
KLF4	5’-ACCCTGGGTCTTGAGGAAGT-3	5’-ATGTGTAAGGCGAGGTGGTC-3
36B4	5’-ATCCCTGACGACGCACCGCCGTGA-3	5’-TGCATCTGCTTGGAGCCCACGTT-3

Table S2. Mouse primer sequences used for qRT-PCR

Target (Mouse)	Sense	Anti-sense
Elovl6	5’-CCCGAACTAGGTGACACGAT-3’	5’-TACTCAGCCTTCGTGGCTTT-3’
SCD1	5’-GCTGGGCAGGAACTAGTGAG-3’	5’-GGTAGGGAGGATCTGGAAGC-3’
SMα-actin	5’-AGACAGCTATGTGGGGGATG-3’	5’-GAAGGAATAGCCACGCTCAG-3’
SM22α	5’-TCCAGTCCACAAACGACCAAGC-3’	5’-GAATTGAGCCACCTGTTCCATCTG-3’
p53	5’-ATCTGGACGACAGGCACACT-3’	5’-CTTCGGGTAGCTGGAGTGAG-3’
p21	5’-GTCCAATCCTGGTGATGTCC-3’	5’-CAGGGCAGAGGAAGTACTGG-3’
mTOR	5’-CATCCCCAAGGTGCTACAGT-3’	5’-CAAACCACAGGGTGAGGACT-3’
KLF4	5’-CAGCTTCATCCTCGTCTTCC-3’	5’-CGGGACTCAGTGTAGGGGTA-3’
36B4	5’-ATCCCTGACGACGCACCGCCGTGA-3	5’-TGCATCTGCTTGGAGCCCACGTT-3

Supplemental References:

1. Gallo R, Padurean A, Toschi V, Bichler J, Fallon JT, Chesebro JH, Fuster V, Badimon JJ. Prolonged thrombin inhibition reduces restenosis after balloon angioplasty in porcine coronary arteries. *Circulation*. 1998; 97:581-588.

2. Lin RY, Reis ED, Dore AT, Lu M, Ghodsi N, Fallon JT, Fisher EA, Vlassara H. Lowering of dietary advanced glycation endproducts (AGE) reduces neointimal formation after arterial injury in genetically hypercholesterolemic mice. *Atherosclerosis*. 2002; 163:303-311.

3. Roque M, Fallon JT, Badimon JJ, Zhang WX, Taubman MB, Reis ED. Mouse model of femoral artery denudation injury associated with the rapid accumulation of adhesion molecules on the luminal surface and recruitment of neutrophils. *Arterioscler Thromb Vasc Biol*. 2000; 20:335-342.

4. Doi H, Iso T, Yamazaki M, Akiyama H, Kanai H, Sato H, Kawai-Kowase K, Tanaka T, Maeno T, Okamoto E, Arai M, Kedes L, Kurabayashi M. HERP1 inhibits myocardin-induced vascular smooth muscle cell differentiation by interfering with SRF binding to CArG box. *Arterioscler Thromb Vasc Biol*. 2005; 25:2328-2334.

5. Tschuch C, Schulz A, Pscherer A, Werft W, Benner A, Hotz-Wagenblatt A, Barrionuevo LS, Lichter P, Mertens D. Off-target effects of siRNA specific for GFP. *BMC Mol Biol*. 2008; 9:60.

6. Farhat MY, Vargas R, Dingaan B, Ramwell PW. In vitro effect of oestradiol on thymidine uptake in pulmonary vascular smooth muscle cell: role of the endothelium. *Br J Pharmacol*. 1992; 107:679-683.

7. Aoyagi-Ikeda K, Maeno T, Matsui H, Ueno M, Hara K, Aoki Y, Aoki F, Shimizu T, Doi H, Kawai-Kowase K, Iso T, Suga T, Arai M, Kurabayashi M. Notch induces myofibroblast differentiation of alveolar epithelial cells via transforming growth factor-{beta}-Smad3 pathway. *Am J Respir Cell Mol*

Biol. 2011; 45:136-144.

8. Bligh EG, Dyer WJ. A rapid method of total lipid extraction and purification. *Can J Biochem Physiol*. 1959; 37:911-917.

Elongation of Long–Chain Fatty Acid Family Member 6 (Elovl6)–Driven Fatty Acid Metabolism Regulates Vascular Smooth Muscle Cell Phenotype Through AMP–Activated Protein Kinase/Krüppel–Like Factor 4 (AMPK/KLF4) Signaling

Hiroaki Sunaga, Hiroki Matsui, Saki Anjo, Mas Risky A. A. Syamsunarno, Norimichi Koitabashi, Tatsuya Iso, Takashi Matsuzaka, Hitoshi Shimano, Tomoyuki Yokoyama and Masahiko Kurabayashi

J Am Heart Assoc. 2016;5:e004014; originally published November 23, 2016;
doi: 10.1161/JAHA.116.004014
The *Journal of the American Heart Association* is published by the American Heart Association, 7272 Greenville Avenue, Dallas, TX 75231
Online ISSN: 2047-9980